

MRI and MRS of the human brain at magnetic fields of 14 T to 20 T: Technical feasibility, safety, and neuroscience horizons



Thomas F. Budinger^{a,*}, Mark D. Bird^b

^a University of California, Berkeley, Lawrence Berkeley National Laboratory, Berkeley, CA, United States

^b National High Magnetic Field laboratory, Florida State University, Tallahassee, FL, United States

A B S T R A C T

The three goals of this paper are: 1) to evaluate the improvements in technology for increasing magnetic flux density (magnetic field) to 14 T in the next few years and eventually to 20 T; 2) to highlight neuroscience opportunities enabled by these advances; and, 3) to evaluate the physiological and biophysical effects associated with MRI at very high performance levels. Substantial recent advances in magnet technology including superconductor developments enable neuroscience goals that are not obtainable at contemporary magnetic fields. Ten areas of brain neuroscience include potential improvements in resolution for functional MRI(BOLD), diffusion weighted MRI, tractography, susceptibility weighted MR, neuronal architecture patterns related to human behavior, proton spectroscopy of small brain biochemicals, chemical exchange saturation transfer (CEST), dynamic contrast enhanced MRI, brain energy metabolism using ¹³C, ¹⁷O, and ³¹P; and brain electrolyte physiology using ²³Na, ³⁵Cl, and ³⁹K.

Physiological phenomena and safety aspects include: absorbed RF power, acoustic sound pressure levels, induced electric fields, Lorentz forces, magnetohydrodynamic forces, and biophysical phenomena in cells and tissues. Where feasible, effects are quantified for magnetic fields beyond 7 T with the conclusion that there are no foreseen barriers either in the technical or human safety aspects of brain MRI and MRS at fields up to 20 T. This conclusion is conditioned on results of recommended experiments to verify the predicted level of physiological effects beyond 9.4 T.

This technology is predicted to enable quantification of biochemical components of the functioning brain not detectable heretofore.

Introduction

The opportunities for research in human brain structure, function and chemistry created by magnetic fields much higher than exist today are tremendous, as many neurophysiology and neuropsychiatric questions cannot be approached by any other methods. This paper gives examples of and goals for neuroscience studies that can be enabled at magnetic fields greater than currently available as well as descriptions of technologies that enable human brain studies at 14 T to 20 T. Beyond 1.5, 3.0, and a few 4 T magnets used for clinical studies, there are fifty, 7 T MRIs, four large bore 9.4 T MRIs (one currently under repair after a quench), one 10.5 T whole body MRI, and two MRIs being installed at 11.7 T.

The prospects for achieving magnets at fields of 14 T to 20 T with bore sizes that will accommodate the human head (e.g., 680 mm) are now good due to technological advances in superconductor materials whose performance in the last few years, along with innovative nested

coil designs, gives confidence for the development of large-bore MRI/MRS brain imaging instruments in a few years. Advances in gradient coils and RF transmit/receive antenna arrays presented in sections below as well as other papers in the present issue (i.e., [Uğurbil, this issue](#), [Winkler et al., this issue](#)) will show that the resolution improvement, signal to noise increases and spectral dispersion advantages of higher fields can be realized without exceeding human safety operating limits of absorbed power, peripheral nerve stimulation, noise and other physiological effects.

The rationale for an investment in research sites that can provide neuroscience research at 14 T and above is that MRI and MRS at these fields can provide scientific information of major significance to human biology and human behavioral research. But advancement of magnetic resonance in vivo studies to fields two to three times higher than currently available is an engineering and financial challenge. Expectations for major advances in clinical medicine have already been realized from results at the more than 50 institutions with 7 T

* Corresponding author.

E-mail addresses: tbudinger@lbl.gov (T.F. Budinger), bird@magnet.fsu.edu (M.D. Bird).

MRI capabilities. For example, regional brain inflammation foci are detected that are not visualized at lower fields (e.g., [Sinnecker et al., 2015](#); [Trattinig et al., 2016](#)) and abnormalities of the right dentate nucleus in schizophrenia have been detected reliably for the first time ([Kirov et al., 2013](#)).

The following is a list of pioneering neuroscience goals that provide the impetus for pursuing this project and provide the rationale for a major endeavor to increase the capabilities of MRI and MRS for human brain studies:

- fMRI with resolution volumes less than 0.1 μL at 20 T.
- Neuronal networks at less than 0.2 mm resolution.
- Local brain architecture at 0.05 mm resolution using susceptibility-weighted MRI.
- Relationships between functional patterns and mental disorders.
- Biochemistry aberrations associated with behavioral disorders.
- Brain activity and plasticity revealed by chemical exchange saturation transfer (CEST).
- Mapping of the Na/K ATPase using dynamic contrast enhanced fMRI.
- Mapping of regional glucose oxidation using the ^{13}C bicarbonate signal.
- Quantification of brain bioenergetics using ^{31}P MRS.
- Oxygen consumption by $^{17}\text{O}_2$ MRS with a 6.7 SNR increase from that at 7 T.
- Role of sodium MRI in homeostasis related to aging.
- Determination of quadrupolar nuclei (Na, Cl, K) concentrations to reflect membrane potentials related to mental states.

Expansion and support for the above topics are given in [Section 4](#) of this paper.

The quantitative projections for improvements in resolution, SNR, safety and specific neuroscience applications are expansions of a previous review of the magnet technologies, applications, and safety in reaching 14 T to 20 T ([Budinger et al., 2016](#)). Discussions regarding expectations and limits for SNR and contrast to noise ratio benefits to medical science at higher fields than are currently available have also been reviewed by [Duyn \(2012\)](#), and the evolution of functional MRI by [Uğurbil, \(this issue\)](#).

Sections of this paper include: 1) Introduction; 2) sensitivity improvements with field and RF technologies; 3) superconducting magnet engineering advances that enable the neuroscience opportunities; 4) neuroscience opportunities including MRI and MRS resolution improvements, 5) physiological effects and safety, and 6) Summary.

Signal to noise improvements and RF technologies

The achievable signal-to-noise ratio (SNR) for the detection of magnetic resonance signal depends on magnetic field strength (B), longitudinal relaxation time (T₁), T₂* and the RF coil quality factor (Q):

$$\text{SNR} \propto B^\beta (Q \times (T_2^*/T_1))^{1/2} \quad (1)$$

The constant β varies from 1 to 2 and is close to 1.75 as predicted by [Hoult and Richards \(1976\)](#). The expected improvements in sensitivity for imaging are mainly from increases in the magnetic field, B, but the RF generation technology can be a significant factor in achieving improved SNR for both MRI and MRS. In addition, image quality and quantitative accuracy depend on the shim coil hardware ([Stockmann and Wald, this issue](#)), and performance of the gradient coils ([Winkler et al., this issue](#)). This section presents the recent analyses of SNR expectations for increasing fields to 20 T. Also presented is a SNR analysis for different transmit and receive coils. Considerations of the penalties of absorbed power are given in the RF power deposition, Specific Absorbed Power (SAR) section below.

Signal to noise increases with B₀

The major advantages are increases in sensitivity and spectral dispersion as well as improved visibility of specific biomolecules obscured by signals from nearby metabolites and tissue water discussed below. Recent measurements up to 9.4 T for the human head with multichannel array receivers suggest a SNR increase that scales as $B_0^{1.65}$ for protons ([Pohmann et al., 2016](#)) close to the predictions of [Hoult and Richards \(1976\)](#) of a 7/4th power increase. Measurements of SNR gains above 9.4 T will depend on the imaging sequence and the influence of relaxation parameters. For proton MRI, simulations show more of a linear relationship with field increases beyond 9.4 T ([Cao et al., 2015](#)), and measurements in the rodent brain show a slightly better than linear gain of SNR with a field increase from 9.4 T to 21.1 T ([Schepkin, 2016](#)). The SNR gains for surface coil applications to in vivo chemical spectroscopy have been shown to increase much more than linearly with field in simulations and measurements at Berkeley, California many years ago ([Keltner et al., 1991](#)) and confirmed recently ([Lattanzi et al., 2016](#)). In addition to SNR gains measured for tissue water detection sensitivity, the actual SNR for specific metabolites will include multiplicative factors based on magnetic field effects on contrast, chemical shift dispersion, and relaxation parameters of metabolites and tissue water as well as the gains from innovative RF transmit and receive coils.

Application of longitudinal relaxation enhancement (LRE) ([Shemesh et al., 2013](#)) using selective excitation of metabolites can enable detection of small molecules not detectable at current fields, as demonstrated in animal studies at 21.1 T and shown in [Fig. 1a](#) and discussed further in the Neuroscience Applications section of this paper. Heteronuclear SNR increases with fields beyond 7 T are much greater than linear as shown for ^{17}O in [Fig. 1b](#) ([Zhu et al., 2001](#)) for the SNR increase from 4.7 to 9.4 T and for the SNR increase from 9.4 to 16.4 T ([Lu et al., 2013](#)); and as shown for ^{23}Na ([Schepkin, 2016](#)) as discussed under ^{23}Na MRI in Neuroscience Applications.

Improvement in detection of contrast reagents is expected at high magnetic fields because their field dependent T₁ relaxivity decreases are less than those of brain tissues, and this will allow reliable quantification of enzyme kinetics using dynamic contrast enhancement methods ([Rooney et al., 2015](#)) discussed further in the Neuroscience Applications section.

Signal to noise improvements from RF coil design

The signal to noise advances due to RF coil design innovations over the past few years have substantially modified our expectations for increases in SNR with field strength. RF coil parallel transmit and receive systems are discussed by other papers in this issue. An illustration of the advances is shown in [Fig. 2](#) from the Dan Sodickson, New York University group ([Lattanzi et al., 2016](#)).

Contrast resolution improvements from motion compensation

A principal contributor to noise in all forms of in vivo imaging is the involuntary motion of the body.

For the head, the amplitude of the six degrees of freedom (displacements and rotations) can lead to significant blurring and have amplitudes similar to those achievable at the resolutions associated with 7 T or higher field imaging. These motions are from cardiac activity, respiration, and swallowing. The amplitudes are 42, 74, 138 μm for lateral, anterior/posterior, and head-to-foot, respectively; and rotations are less than 0.04 degrees ([Maclaren et al., 2013](#)). The highest resolution gradient echo MRI images at 7 T have been obtained using the prospective motion correction method, which tracks the head motion by optical methods and continuously updates the pulse sequence to lock the imaging volume to the position of the brain. Use of this method and selective region imaging has allowed selected region

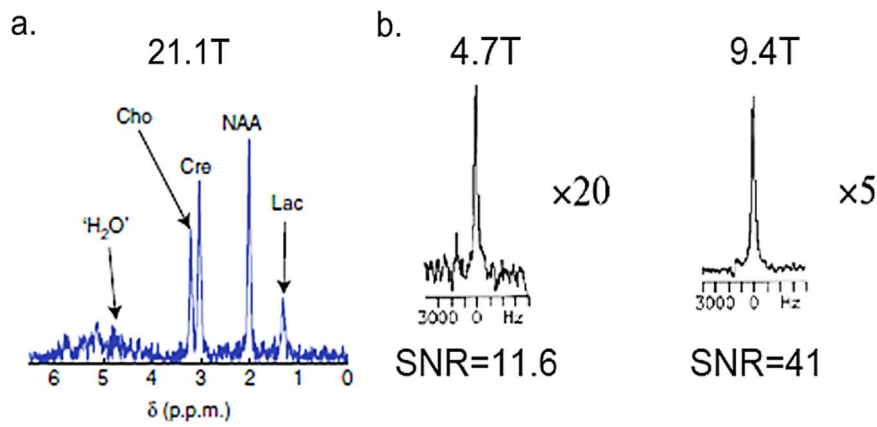


Fig. 1. (a) Signal to noise (SNR) advances facilitated by 21.1 T and the pulse sequence of Longitudinal Relaxation Enhancement for in vivo rodent proton spectroscopy of 50 μ L voxel with 5 s acquisition. The NAA SNR is 50:1, (From Shemesh et al. 2014 with permission). (b) Oxygen-17 spectra from the in vivo rodent brain of 16 μ L voxel with 15 s acquisitions. SNR increases from 4.7 T to 9.4 T, (From Zhu et al.,2001, with permission).

spatial resolution imaging at an isotropic resolution of 0.2 mm for a 3D ToF sequence and acquisitions over one hour (Stucht et al., 2015). Other reports of high nominal resolution studies do not necessarily translate to the image resolution as the nominal resolution based on obtainable pixels is not the true anatomical resolution. The amount of blurring from motion is related to the sequence repetitions necessary and this is related to the obtainable SNR. Higher fields will reduce the time needed to acquire data generally.

Magnet technologies

Human head and whole-body MRI magnets developed to date operate at less than 12 T and use NbTi as the superconducting element (Fig. 3). While it is widely believed in the MRI community that magnet technology precludes development of high field magnets beyond those currently available, higher fields in larger bores not only can be realized but have been, as shown in Table 1. Moving beyond 11.7 T will require Nb₃Sn, which can carry supercurrent at higher fields (up to ~25 T). Magnets beyond ~16 T will require high temperature superconductor (HTS)-based conductors that rely on either ReBCO, Bi2212 or Bi2223 superconductor materials (Re refers to a rare-earth element, typically Y or Gd) (Fig. 3).

Nb₃Sn magnet technology

For magnets in the 12–16 T range, Nb₃Sn is the material of choice for the innermost (high-field) coils. This conductor material is presently used in three types of magnets: persistent small-bore NMR

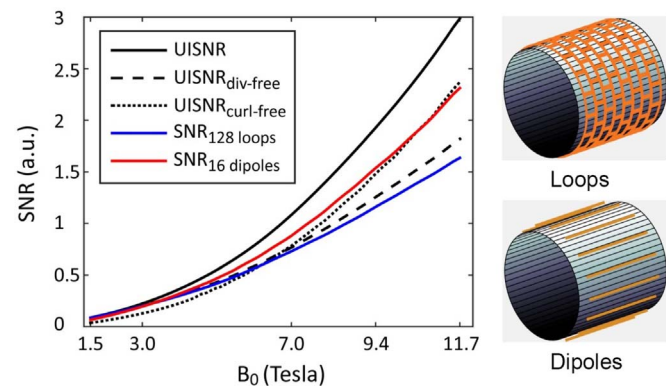


Fig. 2. Demonstration of the SNR expectations for two types of coils, multiple loop arrays, and dipole arrays. The ultimate intrinsic SNR (UISNR) computed from electrodynamic principles is shown vs. B-field for the number of elements in each coil type (From Lattanzi et al., 2017, with permission).

spectrometers up to 23.5 T built by Bruker in Germany; large, high-field magnets providing fields up to 13 T in a 50-cm warm-bore (Smeibidl et al., 2016); and, various high-field, large-bore magnets for condensed-matter physics and fusion experiments (Table 1).

As seen in Fig. 4, the current-density of NbTi at 7 T is ~700 A/mm², while the current-density of Nb₃Sn at 14 T is > 1000 A/mm². The Lorenz forces acting on the conductor are given by $\mathbf{J} \times \mathbf{B}$ (product of

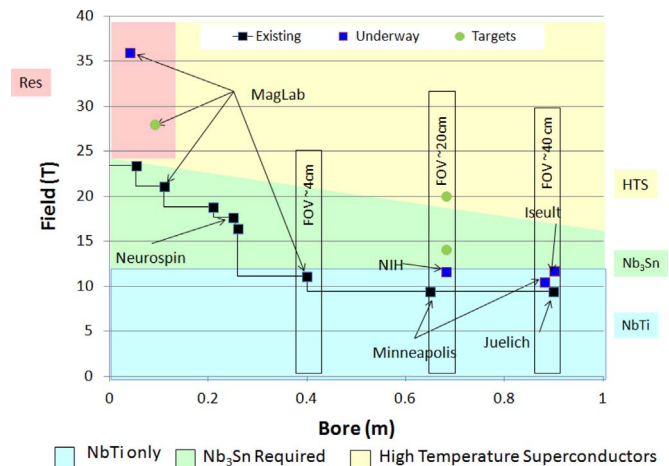


Fig. 3. Important parameters of MRI magnets are shown. Black squares indicate magnets presently in operation. Blue squares indicate magnets presently under construction, repair, or in commissioning. Target designs are shown as green circles. The background colors indicate the different conductors used to construct the magnets.

Table 1

Various non-MRI high-field, large-bore superconducting magnets.

| Location | Field | Bore | Date | Developer |
|---------------------------|-------------------|--------------------|------|--|
| Tokai, Japan | 11.3 T | 158 cm | 2000 | ITER [Martovetsky et al., 2001; Martovetsky, 2015] |
| Tallahassee, FL, USA | 14.1 T | 60 cm | 2000 | MagLab [Miller et al., 1994, Brandt et al., 2001] |
| Berlin, Germany | 13 T ^b | 50 cm | 2014 | MagLab [Dixon et al., 2017] |
| Tallahassee, FL, USA | 13 T ^b | 46 cm | 2016 | MagLab [Bird et al., 2015] |
| Toki, Japan | 13 T | 60 cm ^a | 2017 | NIFS [Imagawa et al., in press] |
| Toki, Japan | 15 T | 50 cm ^a | 2017 | NIFS [Imagawa et al., in press] |
| Nijmegen, The Netherlands | 12 T ^b | 52 cm | 2018 | NHFML/MagLab [den Ouden et al., 2016] |

^a Indicates a magnet built with a cold bore; the indicated dimension is approximately the warm-bore dimension if the magnet were converted.

^b The magnets in Berlin, Tallahassee and Nijmegen are resistive/superconducting hybrids. The data shown above are for the superconducting part only.

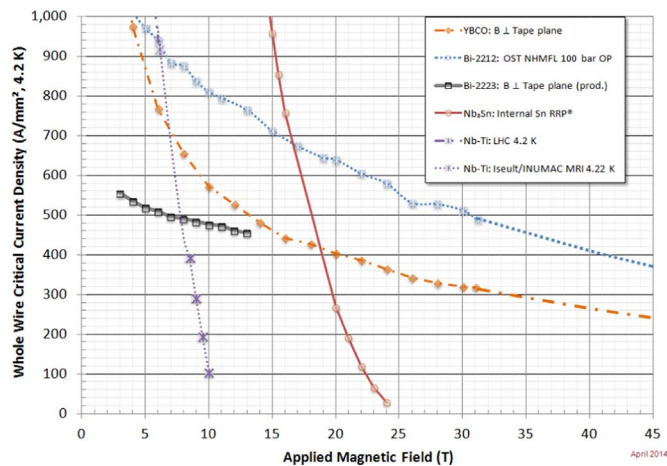


Fig. 4. Maximum current density of superconducting wires operating at 4.2 K as a function of the applied magnetic field. Magnets operating at > 10 T require Nb₃Sn or lower-temperature operation. Magnets operating at > 23 T require High-Temperature Superconducting (HTS) materials.

current-density and magnetic field). Thus, the hoop stress in the 14 T coil will be almost three times that of the 7 T coil. Today's MRI magnets use copper reinforcement (Lvovsky et al., 2013; Vedrine et al., 2010) whereas large, high-field magnets shown in Table 1 above use steel reinforcement, which has five times the strength and twice the stiffness of copper. Consequently, by using Nb₃Sn instead of NbTi and steel reinforcement instead of copper, a 14 T human MRI magnet will be smaller than the largest MRI magnet in development today, the 11.7 T, 90-cm bore Iseult magnet (Bird et al., 2015).

Presently, ultrahigh-field magnets for condensed matter physics (Miller et al., 1994) and NMR (Markiewicz et al., 2000) use multiple nested coils. This allows Nb₃Sn to be used for the high-field regime while less expensive NbTi is used for the low-field regime (< 10 T). In addition the nested coil design allows different ratios of copper to superconductor to be used for different sections of the magnet, and it also allows reduction of the hoop-stress in the inner coils (Wilson, 1983). Human MRI magnets above 3 T already use multiple nested coils (Lvovsky et al., 2013).

As we continue to develop MRI to fields beyond 12 T, it will become appropriate to use Nb₃Sn for the inner coils and NbTi for the outer coils. As shown in Fig. 4, when the field reaches ~17 T, the current-density in the HTS materials starts to exceed that of the Nb₃Sn. Consequently, for magnets in the 20 T range, it might be more cost-effective to build a smaller magnet using expensive HTS materials for the innermost coil than a larger magnet using less-expensive LTS materials exclusively.

HTS magnet technology

While HTS materials have been known since 1986, limitations in strength, current density, and manufacturing processes precluded their use in ultrahigh-field magnets. However, three new conductors have emerged in recent years: SuperPower YBCO tape with 600 MPa strength (Majkic et al., 2010); NHMFL over-pressure-processed isotropic Bi2212 (Larbalestier et al., 2014); and Sumitomo Ni-Cr-reinforced Bi2223 (Nakashima et al., 2015). The incorporation of HTS materials with LTS materials into actively stabilized LTS/HTS duplex designs operating in non-persistent mode promises to open the possibility of human MRI magnets at fields > 16 T. For example, two all-superconducting magnets generating fields of 26 and 27 T have been demonstrated in 2015. A 32 T all-superconducting magnet is being constructed by the National High Magnetic Field Laboratory (MagLab). The design is a combination of five LTS coils with two HTS coils in a serial, concentric assembly (Weijers et al., 2014). The 32 T magnet will be completed for users at the MagLab in 2017.

In addition to the major strides in HTS materials science, there has been a breakthrough in the problem of poor reliability of superconducting connections that are needed for operations in the persistent mode. A high-field magnetic resonance instrument operating in the non-persistent mode was first demonstrated in a 600-MHz (14.1 T) NMR magnet based on Nb₃Sn tape built by Intermagnetics General Corporation for Carnegie-Mellon University in the late 1970s and was more recently re-introduced by the Japanese ultrahigh-field NMR effort in 2009 utilizing LTS and HTS coils at 9.4 and 2.3 T, respectively, running in an ultra-stabilized mode. This NMR spectrometer provided a conventional set of 500 MHz (11.7 T) high-resolution biomolecular NMR spectra despite running non-persistently (Yanagisawa et al., 2008). In early 2016 the Japanese group reached 1020 MHz (23.9 T) with a similar test-coil system (Nishiyama et al., 2015). While these are magnets for NMR spectroscopy studies with narrow bores, they embody a proof of concept that gives confidence that large-bore MRI magnets at > 14 T can be built to operate in the non-persistent mode if necessary.

Using HTS materials, fields exceeding 20 T are possible with a volume suitable for human MRI. The advancements that enable this expectation are: 1) improvements in HTS material performance and reliability; 2) development of magnet technologies using HTS materials at the National High Magnetic Field Laboratory and elsewhere with demonstrated fields over 35 T; and 3) demonstrated use of non-persistent mode operation until the reliability of HTS persistent joints is achieved. Development is still needed to meet the stability and uniformity requirements of MRI.

Large magnets typically use cables instead of single strands of wire (Fig. 5). This results in a magnet capable of sustaining higher current

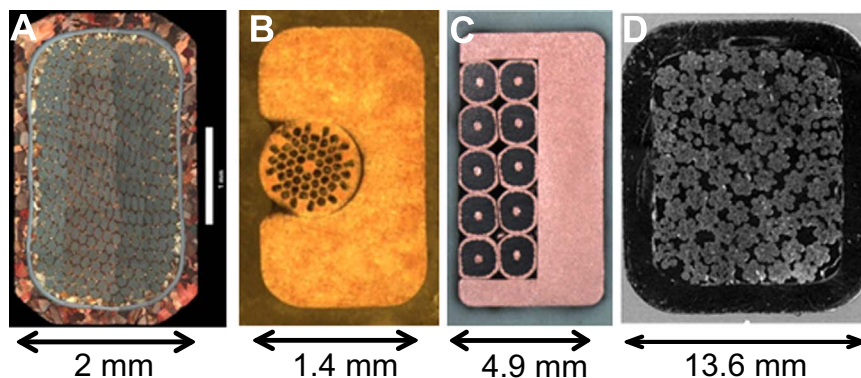


Fig. 5. Conductors used in superconducting magnets. A) Single-strand of Nb₃Sn wire from NHMFL 21.1 T / 10.5 cm NMR magnet; this wire carries 285 A at 21.1 T. B) NbTi Wire-In-Channel for a 1.5 T MRI magnet; this wire can carry ~200 A at 5 T. C) 10-strand NbTi cable with Cu stabilizer and reinforcement designed for 11.75 T / 90 cm magnet under construction by Iseult; this cable can carry 1,500 A @ 12 T. D) 525-strand Nb₃Sn cable with stainless steel reinforcement from NHMFL 45 T hybrid magnet; this cable can carry 10,000 A at 15 T. Photos in B and C courtesy of Hem Kanithi.

Table 2
Conductors for Various MRI Magnets.

| | 3 T, 90 cm | 21 T, 10 cm | 11.74 T, 90 cm (Iseult) | 14 T, 68 cm (proposed) |
|--------------------------------------|------------|--------------------|----------------------------|---------------------------|
| Superconductor | NbTi | Nb ₃ Sn | NbTi | Nb ₃ Sn |
| # of strands | 1 | 1 | 10 | 100 |
| Current (Amps) | ~300 | 285 | 1,500 | 10,000 |
| Reinforcement | Cu | Steel | Cu | Steel |
| Strength (MPa) | > 250 | 1,400 | > 250 | 1,400 |
| Stiffness (GPa) | 110 | 200 | 110 | 200 |
| Stabilizer | Cu | Cu | He | He |
| C _p (mJ/cc/K) | 1 | 1 | 552 | 552 |
| Protection | Cu | Cu | Cu | Cu |
| J _{cu} (A/mm ²) | ~280 | ~230 | ~70 | ~250 |

and lower inductance than use of a single strand, which simplifies protecting the magnet if a quench occurs. To date, all human MRI magnets have used the single-strand approach. The “Iseult” magnet is an 11.7 T MRI magnet being developed as a joint French-German collaboration (Vedrine et al., 2010). This magnet will be the first human MRI magnet to employ NbTi cable. Table 2 compares conductors used for various MRI magnets. As we continue to move into the large-magnet regime to reach higher fields for MRI, Nb₃Sn and HTS cables will be used. While Nb₃Sn cables have been used extensively for high-field condensed-matter physics, fusion, and for accelerator magnets, HTS cables suitable for use at high fields are in their infancy. This is a very active field of research at present with various HTS materials (YBCO, Bi2212, Bi2223) being cabled in a number of configurations in the pursuit of ultrahigh-field large magnets. At present, the accelerator community has been leading the development of Conductor-on-Round-Core using YBCO tape (van der Laan et al., 2015) and the Rutherford cable based on Bi2212 round-wire (Godeke et al., 2008). The fusion community has championed twisted stacks of YBCO tape (Takayasu et al., 2016). It is too early to say which technology will be best suited for MRI beyond 14 T, for the 17–21 T range.

Small animal 28.1 T MRI development

Closely related scientifically to human MRI is the progress on ultrahigh-field condensed-matter NMR and preclinical MRI (small-bore, 1 ppm systems). A 36 T resistive/superconducting hybrid magnet with a 40 mm bore is being completed at the NHMFL (Bird et al., 2015). The magnet is intended to have uniformity and stability of 1 ppm over a 1-cm DSV and be suitable for condensed-matter NMR at 36 T (1.5 GHz) (Li et al., 2011). The bulk of the magnet is Nb₃Sn-based cable-in-conduit-conductor operating at 4.5 K. As indicated in Table 1, this section provides 13 T in a 46-cm bore. The inner high-field section uses copper-based, water-cooled resistive coils. The inner resistive coils can be removed and replaced easily. The resistive coils could be replaced with a set that has a larger bore to provide 28.1 T (1.2 GHz) with a 90 mm bore having 1 ppm over 30 mm DSV. This would be suitable for mouse-brain imaging. Alternatively, HTS magnet technology has advanced to the point that an all-superconducting magnet could be developed for the same purpose. Modifying the hybrid magnet would likely be less expensive than building an entirely new all-superconductor system, while a new system could become commercially available for multiple users.

Initiative to advance NMR and MRI/MRS high magnetic field technologies in the U.S.A

Advances in magnet technologies presented in this section are essential for ultra high field NMR instrumentation used in physics, biology, chemistry and material science, as well as MRI and MRS for advanced human brain studies. The needs were recognized in a National Research Council Report (2013) with recommendations that

led to a national workshop sponsored by the National Science Foundation, the National Institutes of Health and the Department of Energy in November 2015 (Polenova and Budinger 2016). That workshop initiated the current development of a road map to enable establishment of national facilities for advancement of ultra high field NMR and MRI/MRS facilities.

Neuroscience applications enabled by UHF beyond 14 T

In addition to providing methods of increased sensitivity for functional imaging and neuronal architecture and connectivity of the human brain, the increase in sensitivity and spectral dispersion increase of a factor of 2 to 3 over contemporary 7 T MRI allow access to metabolite concentrations in the normal and dysfunctional brain not possible at current fields. Examples of new opportunities are given below. The opportunities are for neuroscience and neuropathology investigative work and not at this time for translational clinical opportunities. Six questions listed below give examples of the type of investigations that can be approached with much higher fields than currently available:

1. How do the patterns of neuronal connectivity correlate to human behavioral and psychiatric problems such as: depression, schizophrenia, autism, dyslexia, Tourette's syndrome, obsessive-compulsive and attention deficit disorders?
2. Are there specific metabolite concentration changes (e.g., serine, glycine, folate, glutamate, possibly some bioamines and methionine) that will become detectable by proton MRS at fields 2 to 3 times higher than available currently?
3. Does fMRI representing Na-K-ATPase kinetics show relationships to nutrition, sleep deprivation, abnormal psychiatric conditions, and dementia?
4. Are there specific regional changes in the chemical composition of mid- brain regions related to the short and long term consequences of brain trauma?
5. Is the regional membrane potential inferred from electrolyte intra- and extracellular average concentrations related to human mental disorders?
6. Can the relative regional fluxes in glucose metabolic pathways show the effects of brain stimulants such as cocaine and amphetamines?

Functional MRI (fMRI) BOLD

The non-invasive nature of the MRI experiment, and the concomitant acquisition of superimposed high-resolution brain anatomy, led to the development of functional MRI (fMRI) (Ogawa et al., 1992). fMRI in its original inception maps the local changes in magnetism when the oxygenation and volume of local blood change in response to a sensory or cognitive stimulation (Uğurbil et al., 1999). This blood oxygen level detection (BOLD) method of fMRI became the principal tool for human cognitive neuroscience and the means by which distributed brain function in human subjects is evaluated both clinically and in brain neuroscience. An historical account of the development and applications of fMRI BOLD is given by Uğurbil, (this issue).

A decade ago the expected BOLD fMRI resolution was at the level of 2 mm at a time when gradient echo based acquisitions were used (Turner, 2002). Since 2007, numerous columnar and layer-specific structures of the human brain with spatial features much less than a millimeter have been mapped by BOLD fMRI. Currently the best isotropic resolution for fMRI using reduced field of view and partially parallel acquisitions is 0.65 mm at 7 T (Heidemann et al., 2012). Since 2007, specific cortical structures with spatial features less than a millimeter have been mapped by BOLD fMRI (Yacoub et al., 2008; Zimmermann et al., 2011; Olman et al., 2012; Gorgolewski et al., 2015; Goa et al., 2014; De Martino et al., 2015; Muckli et al., 2015; Nasr et al., 2016; Setsompop et al., 2016). The techniques used by these

investigators allow approaches to the theoretical physiological spatial resolution dictated by intercapillary distance (~25 μm), and to mapping of cortical layers across the cortical thickness.

Establishment of relationships between brain functions (i.e., visual, somatosensory, memory, etc.) and cellular and local neural circuits will require a major improvement in resolution and optimization of pulse sequence strategies relative to field strength, physiology and vascular architecture (Uludag et al., 2009). The high magnetic field effects on the BOLD signal are complex and depend on whether spin echo (SE) or gradient echo (GRE) sequences are used. For example, the frequency shift across tissue/capillary boundaries is proportional to the product of the deoxygenation level and the magnetic field magnitude. As the field increases there is a micro-vascular weighting because the intra-vascular effects increase with field at least for spin echo MRI. These observations and theoretical validations through modeling have demonstrated that intra-vascular and extra-vascular signal contributions vary not only with field strength, but with diffusion weighting, and the MRI sequence (Duyn and Schenck, 2016). Relaxation parameters change with field and with pulse sequence at specific fields. Uludağ and co-workers have shown how knowledge of these changes can be used to optimize the strategy for fMRI, (BOLD) at ultrahigh fields at and beyond 14 T (Uludag et al., 2009). The Uludağ integrative model can be used to predict what can be expected at 20 T. Their evaluations were made to 16.4 T. An extrapolation from their work to a field of 20 T yields an expected SE T₂ of 18 ms. Though this calculation is only an estimate and extrapolation from previous work, the decrease in T₂ relaxation time with increasing field can be a significant barrier to successful fMRI at fields beyond 14 T.

In order to study ensembles of neurons that perform similar and elementary computations, higher resolution is needed. If we assume linear gains in SNR and BOLD contrast, fMRI at 14 T has the potential for studies at about 0.1 μL voxel volume. This resolution would allow sampling the different cortical layers defined by the neuron types across the cortical thickness (cf. Uğurbil, this issue). We anticipate that at magnetic fields in excess of 14 T, in vivo measurements at a voxel resolution of ~0.05 μL will be feasible. RF penetration for proton imaging is not expected to be a barrier based on developments in RF coils and data acquisition/analysis strategies (Lattanzi et al., 2009; Winter and Niendorf, 2016). With increase in magnetic field the physiological signal increases as does the physiological noise variance and this noise source predominates the signal leading to false positives in fMRI parametric image evaluations. An attractive strategy to mitigate this problem is to acquire the high resolution fMRI using high magnetic fields and multi-coil arrays. This can give data with thermal noise dominance such that the ratio of variances of physiological noise to thermal noise is less than 1.0. As shown by Wald and Polimeni (2016), this could be achieved using highly accelerated, high spatial resolution acquisitions. At 7 T, where physiological noise levels are increased substantially compared to those at 3 T, fMRI data measured using 32-channel array coils are thermal noise dominated when acquired with a modest resolution of $1 \times 1 \times 1 \text{ mm}^3$, especially when using the parallel imaging acceleration typically needed to achieve this resolution for BOLD weighted fMRI.

Diffusion Magnetic Resonance Imaging (dMRI)

Water diffusion-driven displacement distributions reflect structural features and geometric organization of neural tissues. In a water solution, 95% of molecules will travel less than a cell diameter of about 30 μm within 30 ms, but in tissues the diffusion coefficient will decrease because the molecules collide with membranes, fibers and macromolecules. Thus the actual diffusion distance is reduced in biological tissues compared to free water. Over 30 years ago the first MRI images representing a parameter of water diffusion were presented (Le Bihan et al., 1986) and since that time the techniques of diffusion weighted imaging also known as tractography have become a

major clinical and neuroscience investigative tool (Le Bihan and Johansen-Berg, 2012). For example, dMRI has provided clinicians with anatomical localization of and information on temporal changes in stroke, and has given neuroscientists a means for mapping neuronal connections by the ability to image white matter tracts in vivo in the normal and abnormal brain. The methods of tractography have allowed detection of neuronal networks related to neuropsychiatric disorders, congenital abnormalities, and the consequences of brain injuries as well as the plasticity of the human brain. The prospects for continued advances in neuroscience were described recently (Iima and Le Bihan, 2015). Advances of major importance can be expected from magnetic fields of 14 T but these advances require improvements in gradients beyond 100 mT/m and pulse sequence optimization as have been developed for the human Connectome project (McNab et al., 2013; Setsompop et al., 2013).

An expected benefit of the improvement in sensitivity of high magnetic fields is the deployment of diffusion weighted MR spectroscopy as shown in studies of changes of the apparent diffusion coefficient for creatine, n-acetyl aspartate and choline upon visual stimulation in human subjects (Branzoli et al., 2013). The influence of magnetic fields on viscosity, hydration of electrolytes and other and hydrogen bonding is only partly known (cf. Cai et al., 2009). These changes might be important in the interpretation of results from fields of 14 to 20 T.

Tractography

Diffusion weighted imaging (dMRI) led to tractography which provides an unique view of white matter in the brain through measurement of restricted translational diffusion of water by the axons (Basser and Pierpaoli, 2011; Jones et al., 2013) and provides a structural correlate to function connectivity derived from fMRI. dMRI in clinical scanners (up to 3 T) has a spatial resolution limit of about 2 mm, so fiber tracking with dMRI resolves only large bundles of white matter axons. The complex fibrous structure of white matter can be further resolved using methods of high angular resolution diffusion weighted imaging (HARDI) to determine the water displacement probability function (Tuch et al., 2002). Diffusion weighted imaging (dMRI) for tractography with 1 mm isotropic resolution and full brain coverage resolution is feasible (Vu et al., 2015) and 0.65 mm isotropic partial brain coverage has been reported (Heidemann et al., 2012). But important small fibers, which require spatial resolution $\leq 0.5 \text{ mm}$, cannot be resolved. Higher resolution studies using brain stem tissues ex vivo at 11.1 T point to the requirement of isotropic resolution of 0.33 mm to resolve important small fibers (Ford et al., 2013). A major achievement in tractography showing fibrous pathways in a resected human hippocampus with 0.22 mm isotropic resolution was made at the Univ. of Florida 17.6 T MRI/S magnet (Colon-Perez et al., 2015). A fresh surgically-resected anterior temporal lobe section containing the hippocampus of an epileptic patient was imaged for 5 h with a maximum diffusion gradient of 394 mT/m and an echo time of 28 ms (Fig. 6). In principle, resolution of $< 0.3 \text{ mm}$ should be achievable at fields of 14 T and greater. The importance of achieving much better resolution than available in the past is demonstrated by the discovery of previously unknown neurite orientations in the human cortex using cadaver samples at 9.4 T and a gradient of 1500 mT/m (Leuze et al., 2014). The expectation is not to achieve gradients of this amplitude, but to open the horizon for neuronal architectural detail not available at the current SNR achievable with contemporary magnets.

A major engineering task is the development of gradient coils for high gradient operations in a high-field magnet (Winkler et al., this issue). Preliminary successes in current experiments at 7 T and beyond along with parallel acquisition with RF shimming and compressed sense strategies (Setsompop et al., 2008; Setsompop et al., 2016; Stockmann and Wald, this issue) give promise for dMRI at fields of 14 T and higher. Because of the expected loss in sensitivity due to T₂ shortening with field increases, the echo times required will need to be

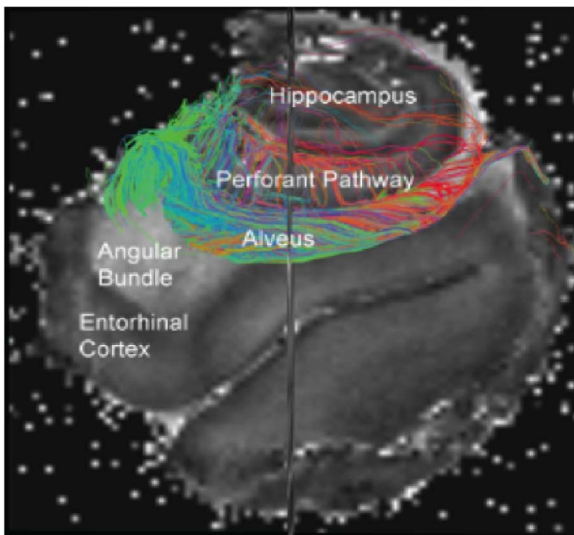


Fig. 6. DTI tractography data superposed on a proton image obtained at 17.6 T from a freshly excised human hippocampus obtained from epilepsy surgery. (From Prof. Thomas Mareci, Univ. Florida, Gainesville).

shorter than those used in the experiments shown in Fig. 6. Gradient coil hardware developments including gradient pulse waveforms optimization are needed to enable tractography at 20 T. With the target of minimizing the current loop parameter, it should be possible to perform studies with gradient magnitudes of 300 mT/m with slew rates controlled by current densities to be determined (e.g., 30 $\mu\text{A}/\text{cm}^2$) as discussed below in sections on peripheral nerve stimulation and brain electrical stimulation.

Magnetic susceptibility-weighted MRI

The phase changes ($\Delta\Phi$) associated with susceptibility differences $\Delta\chi$ lead to well-known image distortions particularly near bone/tissue interfaces. The phase change will increase with field and is proportional to $\Delta\chi \times B_0$. Methods for compensation of these distortions have been developed for imaging the human head at 7 T and samples of much smaller volume at 21.1 T. T_2 shortening with increase in B_0 can lead to serious image distortions particularly in the caudate nucleus, putamen, and globus pallidus where significant iron deposits accumulate with age. However, an evaluation of the dependence of T_2 shortening on increases in field from 0.5 to 4.7 T showed the dependence was not quadratic and had a marked leveling off at higher field strengths. This magnetism saturation can be explained by anti-ferromagnetism and super-paramagnetism of the ferritin core (Bizzi et al., 1990).

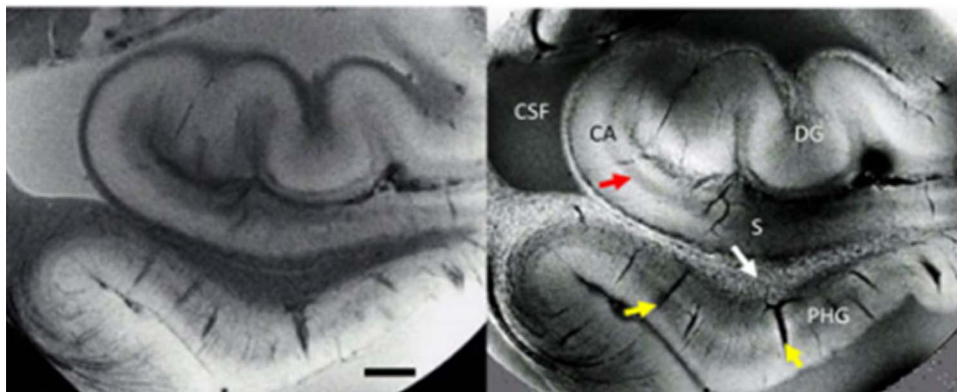


Fig. 7. Susceptibility-weighted MRI of ex vivo hippocampal tissue. Signal amplitude (left) and phase (right) show distinctly different contrast. The dentate gyrus (DG), cornu ammonis (CA), subiculum (S) and parahippocampal gyrus (PHG) are readily identifiable. Contrast noted around vessels (yellow arrows), pyramidal cell layers (red arrow) and in white matter (speckles). Measurements performed at 7 T (TE = 30 ms; resolution, $50 \times 50 \times 500 \mu\text{m}^3$). Scale bar, 2 mm. (From Duyn and Schenck, 2016, with permission).

Instead of a deterrent to high magnetic field anatomical imaging, the differences in susceptibility can be exploited and have led to the highest resolution images of regions of the human brain based on susceptibility differences. Gradient-echo MRI at high fields can provide anatomical information and detection of architectures with better resolution than available by other techniques. The susceptibility differences in tissues based on the presence of iron containing molecules, myelin, and indeed the state of oxygenation of hemoglobin have led to a form of imaging known as susceptibility-weighted (SW) MRI over the last 9 years (Duyn et al., 2007; Haacke et al., 2009). The contrast mechanisms and arguments for improvements in image resolution achievable with increase in field are reviewed in detail by Duyn and Schenck (2016). The magnitude of frequency shifts can be up to 100 Hz at 7 T and the SW MRI can detect shifts as small as 0.1 Hz (Duyn et al., 2007). SW MRI potentials are increased with field increases and open the potential for brain structural studies not possible in the past. For example, the details of the tissue changes in chronic traumatic encephalopathy should be detectable in vivo using SW MRI at ultrahigh magnetic fields. An example of the fidelity obtainable is shown in Fig. 7 based on a gradient echo study (TE 30 ms) at 7 T.

The highest spatial resolution signals from the human brain were obtained by exploiting phase signals from gradient-echo MRI and a multichannel detector at 7 T (Duyn et al., 2007). The nominal voxel size was $0.24 \times 0.24 \times 1 \text{ mm}^3$ (58 nl). The contrast to noise ratio (CNR) is better than can be expected from signal magnitude imaging. Due to susceptibility anisotropy, the phase signals are field-direction dependent and associated with tissue composition (e.g., iron containing molecular layers) (Duyn and Schenck, 2016). Spatial resolution and detection sensitivity might allow semi-quantitative mapping of the distribution of aggregated proteins based on susceptibility anisotropy (e.g., amyloid plaques and phosphorylated Tau protein) even though these aggregations are in the size range less than 100 μm .

Neuronal architecture and functional changes related to human behavior

The microstructural patterns seen at autopsy in the human brains from individuals with psychiatric disorders including PTSD, schizophrenia, depression, autism, chronic traumatic encephalopathy, etc. can to some extent be evaluated during life as evidenced by MRI imaging studies that have demonstrated structural and functional connectivity patterns related to cognitive and behavioral deviations from the norm (Barch et al., 2013). There is a growing literature showing examples of aberrant patterns of connectivity related to depression (e.g., Tao et al., 2013; Guo et al., 2015), and schizophrenia (Cocchi et al., 2014), fMRI in psychopaths (Kiehl et al., 2001), and

fMRI and connectivity studies showing alterations after traumatic brain injury (e.g., Caeyenberghs et al., 2015), and PTSD (Francati et al., 2007). The proposal is not to develop ultrahigh field to make diagnoses in cases of mental disorders, but to provide a method to understand the mechanisms and patterns. There is no question that vital areas of the brain such as the prefrontal cortex, amygdala, hippocampus, putamen, caudate nucleus, cingulate gyrus, and corpus callosum show evidence of anatomical and functional defects in traumatic brain injury even without an unconscious episode. MRI and MRS can provide the research approach to investigate whether some of the 3.5 million pre–high school football players per year will develop brain pathologies later in life (cf. Budinger, 2016). Early detection of functional and architectural changes associated with non-concussive brain trauma using susceptibility weighted MRI discussed above (Duyn and Schenck, 2016) will enable evaluation of a small cohort of young athletes to monitor subtle changes that could result in brain pathologies many years later.

Proton spectroscopy of the human brain at 14–20 T

Spatial distribution and dynamics of small molecules not heretofore measurable can be realized for the first time in human brain neurochemistry studies at fields of 14–20 T. In addition to the enhanced sensitivity and 3-fold increase in spectral dispersion over 7 T, the divergence between the relaxation properties of specific metabolites, background brain tissue and water enable large increases in SNR over that expected from increased fields alone. The large spectral dispersion aids significantly in the suppression of water resonance interferences. We can expect the T_1 for gray matter to increase from 2100 ms at 7 T to 3000 ms at 20 T based on our extrapolations of data from Rooney et al. (2007). But this increase can be mitigated by longitudinal relaxation enhancement (LRE) methods that have realized successes at 9.4 T and 21.1 T (Shemesh et al., 2013). Tailored pulse sequences can enhance detection of metabolites because the relaxation times and the sensitivity from high magnetic fields reinforce one another significantly. When the bulk of the water and macromolecular reservoirs remain essentially unperturbed, the metabolites' T_1 's are shortened by cross-relaxation and/or chemical exchange effects, even in the case of non-labile methyl sites. At 9.4 T LRE effects with up to threefold reductions in apparent T_1 values were observed for resonances in the 6–9 ppm region. In addition, apparent T_1 reductions of 30–50% were observed for several non-exchanging metabolite resonances in the 1–4 ppm region. These LRE effects suggest a novel means of increasing the sensitivity of in vivo experiments (Shemesh, 2013).

Additional benefits at ultrahigh fields are the major shortening of water's T_2 relaxation time relative to metabolites leading to negligible water signals at suitable echo time (TE) experiments. Remarkable improvements to ^1H MRS were demonstrated at 21.1 T in live rodent brains (Fig. 2a) with spectra acquired in 6 s from a 125 μL volumes and a SNR of 50 to 1 (Shemesh et al., 2014). With this unprecedented metabolite SNR, single metabolite diffusion can be determined, thus providing clues into neuronal microstructure that may be obscured due to the contribution of bulk water. By combining highly selective spectral excitations with experiments at very high magnetic fields, ultrahigh-field ^1H spectroscopy of the CNS could become an enabling technology that could map with unprecedented spatial resolution metabolites heretofore not detected by any other method in the living human brain. This can lead to discoveries of new biomarkers of brain function discussed below.

Brain spectroscopic studies of chemical abnormalities in psychiatric disorders

Proton MRS studies in human mental disorders, particularly schizophrenia, have shown alterations in glutamate (10 mM), glutamine (5 mM), gamma amino butyric acid (GABA- 1.5 mM), glutathione

(GSH – 2 mM) and N-acetyl aspartylglutamate (NAAG). The observed metabolite differences between schizophrenic patients and controls depend on brain region, illness stage and medication status (Wijtenburg et al., 2015). The methods use PRESS, STEAM or MEGA-PRESS with J-editing. A principal focus has been on the glutaminergic system due to discoveries by MRS of elevated glutamine in the mid-brain striatum (de la Fuente-Sandoval et al., 2013) and an age-related decline in brain GABA levels (Gao et al., 2013) and concentrations in psychiatric diseases (Wong et al., 2003). There is strong evidence for some dysfunction of the glutaminergic and N-methyl-D-aspartate NMDA receptor systems in schizophrenia (Roland et al., 2005; Errico et al., 2013). The functioning of the NMDA receptor system is dependent on D-serine (e.g., Bardaweel et al., 2014) and glycine and these metabolites, while detectable in the normal brain at 7 T (Choi et al., 2009a,b; Elabyad et al., 2014), will require a much higher field for reliable spectral quantification.

Other metabolites implicated in schizophrenia that might be measured by MRS at fields beyond 7 T are homocysteine and folate (Goff et al., 2004). Folate deficiency has diverse effects on the neurochemistry of mental disorders, as folate functions as a single carbon donor in the synthesis of glycine from serine. Folate is also involved in the synthesis of dopamine, norepinephrine, and serotonin through S-adenosylmethionine methylation pathways. The literature is consistent in reports of reduced levels of plasma folate in schizophrenia and depressive disorder patients (e.g., Saedisomeolia et al., 2014; Goff et al., 2004). But there is as yet no published in vivo proton spectroscopy results for folate.

The complex metabolic pathway of methylation in human biochemistry has been implicated in schizophrenia and there is compelling evidence for dysfunction in this pathway based on a three-fold decrease in the kinetics of methionine metabolism (Sargent et al., 1992). Supporting data from serum and postmortem studies are abnormalities in the concentrations of serine, glycine, folate, methionine, and homocysteine. The potentials of MRS to reveal the dysfunctional elements in the metabolic pathway involving the biomolecules discussed above is a major motivation for establishing a high-field MRI center that will allow in vivo neuroscience investigations for a mental disorder that has a prevalence of 1 in 100 (2.2 million) in the U.S. over age 18 years. The applications of MRS in psychiatry are both in the discovery of the biochemistry of mental illnesses and for monitoring how effective therapies modulate mental and behavioral dysfunction.

Chemical Exchange Saturation Transfer

Chemical Exchange Saturation Transfer (CEST) provides the opportunity to indirectly detect low concentration labile protons, such as protons of amine (NH_2), amides (NH), glucose (glucoCEST), glutamine (gluCEST), glycogen (glycoCEST), urea (urCEST), etc., with greatly enhanced sensitivity. The method proposed in 1998 employs the transfer of magnetization from low concentration metabolic pools of exchangeable protons to water protons and thereby improves detection sensitivity for metabolites such as amino acids, sugars, nucleotides, and heterocyclic ring chemicals (Guivel-Scharen et al., 1998, van Zijl et al., 2007, van Zijl and Yord, 2011). As exchangeable protons have different resonant frequencies from free water, they can be selectively saturated using a metabolite-specific radio-frequency pulse. Due to the exchange between the two pools of protons, saturation can be transferred, leading to a decrease in the free water signal.

CEST benefits greatly from higher magnetic fields due to the increased shift dispersion. This is especially beneficial for the resonances of exchangeable protons, because the shifts are wider than those of the CH, CH₂, and CH₃ protons typically studied in proton MRS. An additional advantage of high field is the lengthening of the T_1 relaxation time of water, allowing a longer duration of the transferred saturation on water protons. The degree of magnification is approximately proportional to $k_{ex}T_1$, where the exchange rate, k_{ex} is the rate

from the exchangeable proton to water. Detection is affected by the exchange regime, requiring k_{ex} to be less than or equal to the shift difference between the two pools of protons. At higher field, the regime shifts to a slower exchange, allowing better visualization of the different exchangeable protons. The increases in SNR, spectral dispersion, and T_1 relaxation lead to a field dependence that is better than linear with B_0 and could be more than quadratic depending on the exchange regime achieved for the particular protons. When coupled to higher-order shims, parallel transmission and reception and other instrumental improvements, this should make it possible to establish in vivo high-resolution maps of certain molecules such as glucose, glycogen or glutamate. A first example of glucose mapping for studying blood brain barrier breakdown in gliomas was recently demonstrated at 7 T (Xu et al., 2015).

CEST does not require inordinately large increases in power over that required for non-CEST imaging and spectroscopy. The actual SAR increase to execute CEST depends upon the proton exchange rate and T_1 times of the species under investigation. Slowly exchanging species require very little power while fast exchanging species require much more power. Many of the endogenous protonated species in exchange with water protons are quite slow, with rates on the order of a 10–100 s^{-1} . Those species can be activated with very weak RF pulses (e.g., 0.6–0.9 μT) as were reported in a human study at 7 T (Jones et al., 2013). New pulsed excitation methods are being developed that do not require saturation of the exchangeable protons and allow editing out of specific proton types in a way similar to multi-dimensional MRS (Van Zijl et al., 2016, van Zijl et al., this issue). The new pulse excitation methods when added to the use of both parallel transmission, simultaneous multi-slice excitation, parallel imaging and compressed sensing, will make CEST techniques easily assessable at much higher fields than currently available.

In summary, the CEST effect shows a marked amplification with magnetic field strength for several reasons including better spectral resolution, a larger range of proton exchanging species amenable for CEST contrast, the increase of water proton T_1 , and the usual increase in sensitivity gained by higher B_0 . Thus, the overall quality of CEST experiments will dramatically increase with B_0 . This has been verified using the NHMFL's 21.1 T system in collaboration with the Univ. of Texas Southwestern group. CEST mapping of protein amide protons in the human brain has been successful at 7 T (Jones et al., 2012). The new low-power pulsed CEST approach in 6 human subjects at 7 T showed that a relayed-Nuclear Overhauser Enhancement CEST effect was about twice as large as the CEST effects downfield and larger in white matter than gray matter (Jones et al., 2013). An extensive treatment of CEST by one of its pioneers is given in a paper in this volume (cf. van Zijl et al., this issue).

CEST measurements with other nuclei (phosphorus CEST) should also be possible at ultrahigh fields. Given that the ^{31}P resonances of ATP, ADP and AMP are resolved at ultrahigh fields, CEST could provide an efficient non-invasive diagnostic tool for quantitative bioenergetic measurements in the human brain.

Dynamic Contrast Enhanced fMRI

Dynamic-Contrast-Enhanced (DCE) methods for mapping trans-capillary water turnover is a minimally invasive MR method consisting of acquiring T_1 -weighted MR images before, during and after IV injection of a gadolinium-based contrast agent (CA). From the kinetics derived from the moment to moment MR signal acquisition data, the mean intracapillary water molecule lifetime can be inferred, with a spatial resolution ≤ 1 mm. Na^+ , K^+ -ATPase (NKA) turnover is proportional to the reciprocal of the intracapillary water lifetime (Rooney et al., 2015). NKA is the brain's most vital enzyme, consuming over 50% of ATP per unit time. Neuronal and neuroglial cells have a metabolic synergy with capillary endothelial cells, and this couples the mean rate constant for equilibrium capillary water molecule efflux,

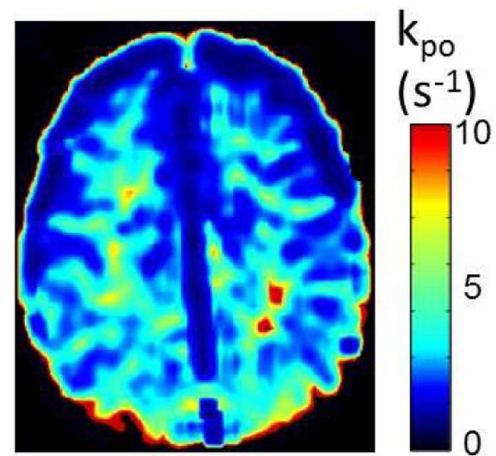


Fig. 8. Parametric image that reflects NKA kinetics in the normal brain. k_{po} is the inverse of intercapillary water turnover. The hot spots may reflect WM tracts connecting cortical “rich club nodes,” which participate in many different transient resting-state functional circuits. (From Rooney et al., 2015, with permission).

k_{po} , to its cell membrane analog, k_{io} that is proportional to NKA turnover (Springer et al., 2014). The first normal human resting-state brain k_{po} map (Fig. 8) was obtained at 7 T (Rooney et al., 2015). Note that NKA activity per capillary is greater in white matter (WM) than in gray matter in the awake human brain. The hot spots may reflect WM tracts connecting cortical “rich club nodes,” which participate in many different transient resting-state functional circuits. Higher field will lead to improved NKA turnover quantification because tissue generic macromolecule relaxivity decreases with the increased field faster than does contrast agent relaxivity (Rooney et al., 2013). Thus, the fractional contrast change increases with B_0 . Fields higher than 7 T will allow a form of fMRI wherein the parameter is not blood oxygenation, or diffusion but NKA enzyme activity.

Functional brain map of glucose oxidation (^{13}C)

Using uniformly labeled ^{13}C glucose infused into human subjects, fluxes on pathways from glucose to pyruvate, pentose phosphate, the TCA cycle, bicarbonate and glutamate have been measured at 7 T with 5 min acquisitions by the University of Texas, Southwestern group (Fig. 9). These whole brain studies can become regional functional mappings at the proposed increase in magnetic fields with almost 10-fold sensitivity increases. Pyruvate is at the branch point in the bioenergetic paths for biosynthesis of amino acids, fatty acids and carbohydrates. A method for mapping the regional fluxes of pyruvate to

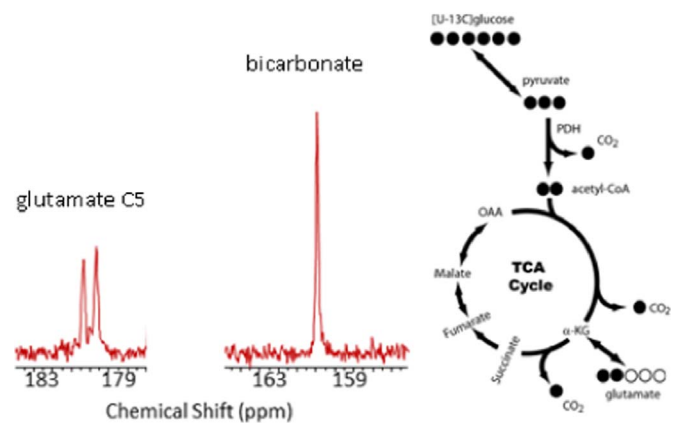


Fig. 9. ^{13}C MRS spectrum of human brain collected in 5 min at 7 T (unlocalized) after i.v. infusion of $[U-^{13}C]$ glucose for 2 h. The spectrum was collected without proton decoupling. Solid circles denote labeled carbon (Univ. of Texas Southwestern group).

specific biochemical products will provide a powerful means of understanding bioenergetic responses triggered by physiochemical changes. Of importance to human behavior is that relative fluxes are known to be affected by brain stimulants such as cocaine (Kiyatkin and Lenoir 2012) and amphetamines (Valvassori et al., 2013). A second powerful use of ^{13}C MRS/MRI at ultrahigh fields is the potential to image glucose oxidation regionally in the human brain. Fig. 9 shows an unlocalized ^{13}C spectrum of the brain after a subject was infused with $[\text{U-}^{13}\text{C}]\text{glucose}$ for 2 h. This spectrum was acquired in 5 min at 7 T without proton decoupling. The glutamate C5 resonance reflects glycolytic conversion of $[\text{U-}^{13}\text{C}]\text{glucose}$ to $[\text{U-}^{13}\text{C}]\text{pyruvate}$ followed by oxidation of pyruvate in the TCA cycle. The strong bicarbonate resonance reflects total oxidation of glucose through the pentose phosphate pathway plus the TCA cycle. If other substrates compete with glucose for energy, this would be reflected in the ratio of glutamate C5 to bicarbonate as measured by MRS. In principle, since this experiment does not require proton decoupling, one should be able to image bicarbonate and use this as a biomarker of regional glucose oxidation in the human brain (Sherry, 2017).

Brain phosphorus bioenergetics and related ^{31}P spectroscopy

Magnetic resonance phosphorus spectroscopy can detect the following ten biochemicals in the human brain. Those involved in the principal bioenergetic reactions with creatine: phosphorus (Pi), phosphocreatine (PCr), adenosine diphosphate (ADP), adenosine triphosphate (ATP); and those that are actively involved in the membrane phospholipid metabolism: uridine diphospho glucose (UDP) (an important precursor for glycogen metabolism), diphospho nicotinamide adenine dinucleotides (NADP) involving oxidative respiratory chains, glycerophosphoethanolamine (GPE), glycerophosphocholine (GPC), phosphoethanolamine (PE) and phosphocholine (PC). Some of these require the improvement in spectral resolution and SNR allowed by 7 T. The improvement in identification of these compounds with increases in magnetic fields, RF coil design and processing methods has been remarkable as all of these peaks can be resolved in vivo.

The SNR and quality of in vivo ^{31}P MRS have improved substantially at 7 T relative to 4 T as shown by comparing values of T_1 , T_2^* and SNR of the phosphocreatine resonance peak acquired from the human occipital lobe (Qiao et al., 2006). The relaxation times decrease and the SNR increases by a factor of 1.56. Dipolar interactions and chemical shift anisotropy influence the PCr longitudinal relaxation time shortening and this decrease with increasing field along with chemical shift dispersion allows shorter repetition times leading to an increase in SNR. These field-based improvements enable resolution of adjacent phosphate metabolite resonance peaks (e.g., $\alpha\text{-ATP}$, NAD, and Pi).

^{31}P spectra from in vivo studies of cat brains at 9.4 and 16.4 T demonstrate the feasibility of quantification of all the important phosphorylated species at ultrahigh fields (Lu et al., 2010). Human brain studies at 9.4 T have shown the ability to map the distribution of the major components of ATP kinetics (Lu et al., 2013). It may also be possible to resolve mitochondrial versus cytosolic ATP and Pi resonances in the human brain at ultrahigh fields. Chemical exchange saturation transfer (^{31}P CEST) could resolve all ATP, ADP and AMP signals and thus become an efficient non-invasive diagnostic tool in quantitative bioenergetic measurements. Acidic (low pH) environments can also be quantified using ^{31}P MRS. At the intermediate frequencies of these nuclei, we do not expect major challenges with respect to RF penetration and homogeneity, as many of these problems are well understood and have been solved from experiences with proton MRI and MRS at 7 T (300 MHz). The frequency of ^{31}P at 11–21 T (190–360 MHz) is on par with proton frequencies at 4.5–8.5 T.

A method for measurement of the kinetics of phosphorus compounds in vivo is by study of the in vivo kinetics of phosphorus compounds through changes in ^{31}P relaxation (T_2) of ^{17}O labeled phosphate. This method that has been successful at low fields (Thelwall

Table 3

Low gamma nuclei available for in vivo studies are listed with average concentrations in vivo and sensitivity relative to ^{23}Na .

20 T, In Vivo MR Signal/Noise Ratio

| Nuclei | Frequency MHz | In vivo AbundanceM | S/N Ratio* |
|---------------|---------------|--------------------|------------|
| Proton-1 | 850 | 94,900 | 1334 |
| Sodium-23 | 225 | 50 | 1 |
| Oxygen-17 | 115 | 18 | 1/3 |
| Rubidium-87 | 278 | 0.6 | 1/6 |
| Chlorine-35 | 83 | 38 | 1/10 |
| Potassium-39 | 40 | 112 | 1/24 |
| Phosphorus-31 | 344 | 10 | 1/37 |
| Deuterium-2 | 130 | 11 | 1/97 |
| Fluorine-19 | 800 | 0.12 | 1/154 |
| Lithium-7 | 330 | 0.5 | 1/456 |
| Nitrogen-15 | 86 | 0.02 | 1/18,500 |
| Carbon-13 | 214 | 0.05 | 1/22,800 |

* ^{13}C and ^{15}N abundance based on 5mM, ^7Li based on clinical levels, T_1 is included

et al., 2007) will be substantially benefitted from improved sensitivity of phosphorous detection at higher fields.

Brain studies using oxygen, sodium, potassium, and chlorine

^{17}O , ^{23}Na , ^{35}Cl and ^{39}K have a very low gyromagnetic ratios and short relaxation times relative to those of protons, ^{13}C and ^{31}P . Thus as shown in Table 3. The SNR for ^{23}Na is 1334 times lower than for protons; ^{17}O is 3 times lower than ^{23}Na ; for ^{35}Cl , 10 times lower than ^{23}Na ; and for ^{39}K , 24 times lower than ^{23}Na (Table 3). The signal to noise calculations of Table 3 made by Victor Schepkin of NHMFL, Tallahassee, include the gyromagnetic ratio and the respective relaxation times. In addition these nuclei have interactions with the electric fields of macromolecules within tissues with a resultant modification of the relaxation times depending on the local concentration of macromolecules (e.g. intracellular relaxation times will be shorter than extracellular relaxation times). Generally, image contrast for ^1H -MRI is determined by the nuclear relaxation properties of the regional tissue water, diffusion anisotropy and susceptibility of the tissue components; whereas MRI and MRS of these other elements give information regarding their concentration as well as the relaxation dependent information about the environment related to intracellular to extracellular macromolecular interactions. Below we give the status of current studies including projections for ^{17}O and ^{23}Na SNR increases for fields to 20 T.

^{17}O MRI and MRS

Oxygen-17, magnetic resonance from endogenous or injected as $^{17}\text{O}_2$ gas or H_2^{17}O opens the opportunity for in vivo studies of oxidative metabolism of the human brain. Oxygen utilization can be a functional imaging parameter that is directly linked to the metabolic processes that subserve neuronal activity (cf. Gordji-Nejad et al., 2014). But ^{17}O nucleus has a spin of 5/2 with a natural abundance of only 0.037%, which results in a H_2^{17}O concentration of 18 mM and a tissue $^{17}\text{O}_2$ concentration of only 1 micromolar for an O_2 partial pressure of 50 mm Hg. Yet static images of ^{17}O distribution in the human brain have been successfully achieved at 7 T. Dynamic changes of metabolism have been measured based on the appearance of H_2^{17}O resonances at 7 T and 9.4 T in the human brain following inhalation of $^{17}\text{O}_2$ enriched gas (Atkinson et al., 2010b; Hoffmann et al., 2011). At higher fields increases in SNR will allow measurements of the regional cerebral

metabolic rate of oxygen consumption. The relaxation times (T_1 , T_2 and T_2^*) of ^{17}O are relatively short, and these relaxation times do increase somewhat with field increase as shown at fields to 9.4 T (Zhu et al., 2001, 2005, 2009) and at 17.6 T (Thelwall et al., 2003). A comparison of ^{17}O MR relaxation times for saline 0.45% between 9.4 T (Zhu et al. 2001) and 21.1 T (Schepkin 2016) shows both relaxation times are longer at 21.1 T ($T_1 = 7.6 \pm 0.24$ ms, $T_2 = 6.5 \pm 0.2$ ms) than at 9.4 T ($T_1 = 6.5$ ms, $T_2 = 4.1$ ms). The ^{17}O quadrupolar moment can interact with local electric field gradients and the temporal fluctuations of this interaction induced by molecular motion dominate the relaxation processes and determine both T_1 and T_2 of H_2^{17}O . The importance of relaxation parameters associated with ^{17}O is seen from the SNR relationship in Eq. (1). As these parameters have a small dependence on magnetic field one can scale the expected signal to noise increase from 7 T to 20 T based on the measured increase of 3.53 in going from 4.7 T to 9.4 T (Fig. 1b). The SNR increase from 7 T to 20 T would be 6.7.

Imaging cerebral oxygen extraction rates during human brain function could provide quantitative regional measures of cognitive performance across the neural network being stimulated analogous to ^{15}O positron emission tomography. These measurements should be feasible at fields ≥ 14 T based on previous experiments at 9.4 T (Atkinson et al., 2010b). The quantitative accuracy, spatial resolution, noninvasiveness and specificity make this functional imaging method superior to positron tomography with ^{15}O . The expense of molecular $^{17}\text{O}_2$ is a drawback and the limited availability of magnetic fields at and above 14 T for clinical studies will keep this method in the research realm. Nevertheless, studies that combine MRI determined perfusion, oxygen utilization, phosphorylation potential (ATP/ADP*PI), and carbohydrate/FFA flux can provide a more complete picture of brain metabolism under different states of brain activity than has existed in the past.

^{23}Na MRI

For 30 years there have been attempts to quantify sodium concentration distributions in the normal and diseased human brain but due to very short relaxation times and low sensitivity there has been little progress until Keith Thulborn pioneered a 9.4 T whole body magnet specifically for studies of sodium and oxygen (Thulborn, this issue). The current performance at 9.4 T for human brain total sodium concentration imaging is 2.5 mm isotropic resolution for 6 contiguous sagittal slices acquired in 10 minutes (Thulborn et al., 2016).

The current capabilities allow quantification of tissue sodium concentration (TSC) and the related parameter of cell volume fraction (CVF) in the human brain (Thulborn et al., 2016). From the 9.4 T studies that showed cell density stability in spite of a shrinking brain volume with age, Thulborn has hypothesized that CVF plays the role of maintaining ion homeostasis including ion gradients. This hypothesis can be tested using cerebral metabolic rate of oxygen consumption (CMRO_2) as measured by ^{17}O MRI but higher fields than 9.4 T are needed.

The SNR is expected to increase by a factor of 6 from 7 T to 21 T. This reflects a 36-fold decrease in acquisition time based on the theoretical prediction of the $7/4$ power dependence of field strength (Hoult and Richards, 1976). Measurements at 21.1 T in the rodent brain show a slightly better than a linear gain of SNR with field increases from 9.4 to 21.1 T. Overall SNR at 21.1 T increases by a factor of 30 from 3 T to 21.1 (Schepkin, 2016).

^{35}Cl MRI

The first in vivo MRI studies that showed the distribution of chloride were done in the rodent at 9.4 T (Kirsch et al., 2010), wherein both sodium, chloride, and proton MRI imaging studies were performed in study durations of 2 h. The relaxation times: T_1 (1.7 ms fast and 25 ms slow) and T_2 (1.3 ms fast and 11.8 ms slow) are very short but longer than observed in phantom and human subjects performed at

7 T. Successful chloride imaging has been performed in the human brain with imaging times of 10 min. even though measurements showed a SNR 15-fold less than sodium (Nagel et al., 2014). Short TE MRI can provide concentrations representative of the 10–15 mM intracellular [Cl].

^{39}K MRI

^{39}K MRI experiments have been carried out at 7 T (Umatham et al., 2013), and at 9.4 T (Atkinson et al., 2014). Evaluation of potassium is hindered by both the low sensitivity (SNR is 24 times less than Na SNR), and by the very short T_2 and T_2^* associated with the quadrupolar interactions from the intracellular potassium as well as interactions with extracellular macromolecules (Nagel et al., 2016). The volume resolution was 1000 μL with an SNR of 5.2 and an image acquisition of 10 min for the human brain. The promise for potassium detection to benefit neuroscience perhaps lies in methods to exploit the quadrupolar interactions of the intra- vs. extracellular potassium ions through multiple quantum detection strategies but the sensitivity might be too low for reliable results even at 20 T for human subjects.

Feasibility of imaging sodium and chloride ion gradients

A major opportunity is the possibility for quantification of electrochemical gradients within different tissue regions of the human brain. The improved SNR of higher fields can enable estimates of intra- and extra-cellular concentrations and the associated gradients that maintain the electrochemical membrane potentials in the brain. The quadrupolar interactions of these ions leads to spectral shifts and spin interactions that can be detected, using tailored RF pulse sequences that are representative of intracellular and extracellular concentrations without using exogenous chemical shift agents. The membrane potential can be computed by a constant times the logarithm of the sum of extra/intra [Na], intra/extra [Cl], and extra/intra [K] ratios modified by respective permeabilities. Even without including [K] the concept can provide a metric of membrane potentials. Even if we can estimate the intracellular concentrations and use peripheral blood for the estimate of extra-cellular concentrations, the approach has potential as was demonstrated for ^{35}Cl in the human brain at 7 T (Nagel et al., 2014; Fleysler et al., 2013) and for both ^{23}Na and ^{39}K in the rodent at 21.1 T (Schepkin et al., 2015; Nagel et al., 2016). The spectra of Fig. 10 represent different in vivo electric field gradient environments and are related to intracellular and extracellular compartments but not necessarily proportional to the sodium and potassium concentrations. Previous experiments in the beating rodent heart validated the concentration values from NMR against chemical assays (Schepkin et al., 1998). This validation also will be required in the brain. The sensitivity increase needed to apply this approach to the human brain will require fields beyond 14 T based on the increase in noise from the difference in size between rodent and human brains (Macovski, 1996) unless surface coils or other reduced volume selection strategy is used.

Physiological effects and safety at 14 T and above

Background

The physiological effects associated with high magnetic field MRI and MRS discussed previously (Budinger et al., 2016) is expanded in this section with substantially new information on acoustic sound levels, specific absorbed power limitations, quantification of forces, expected current densities associated with gradients planned for MRI and MRS applications and the inclusion of magnetic field effects on free radical lifetime prolongation. The first scientific papers on physiologic phenomena and potential health effects that might be caused by MRI and MRS appeared almost 40 years ago (Budinger, 1979; Wolff et al., 1980). These papers focused on predicted physiological effects of RF heating, peripheral nerve stimulation, thresholds for turning torque on molecular assemblages, and possible genotoxic effects noted in biologic

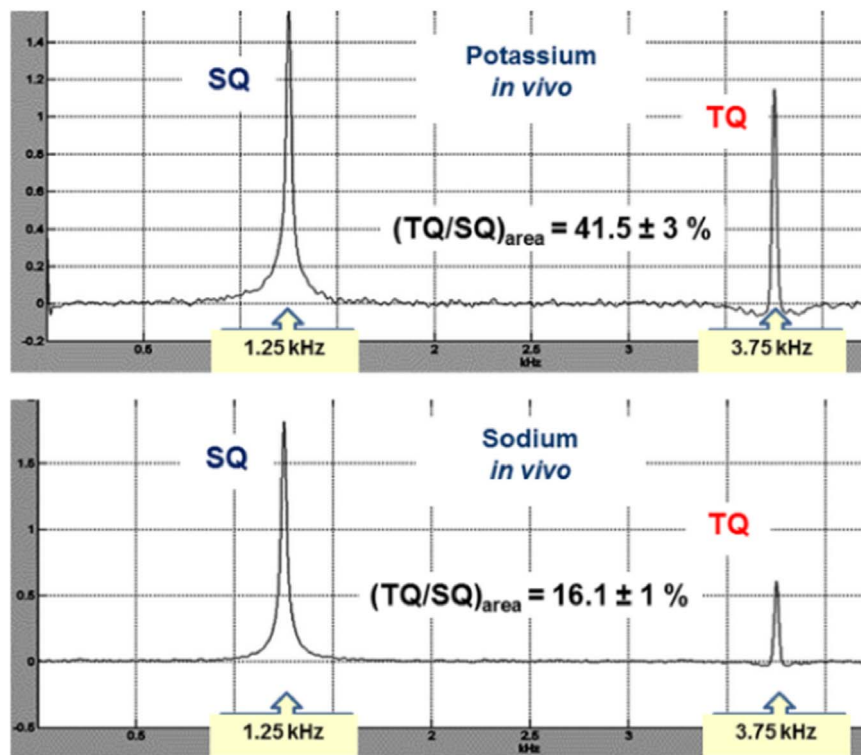


Fig. 10. Detection of sodium and potassium in the rodent head in vivo. The two peaks in each spectrum represent the signal from different electric potential regions of the tissues. In the case of sodium, the concentration ratios correspond to total head sodium for the single quantum (SQ) peak and to intracellular sodium concentration for the triple quantum (TQ) peak. In the case of the potassium, the TQ peak arises mainly from the total intracellular potassium. Each is from the QTTPPI pulse sequence (Schepkin et al., 2015).

cell cultures exposed for long durations at relatively low fields. Over the past decades of human subject observations, animal studies and cell or tissue culture experiments, there have been specific symptoms reported from human subjects and some tissue and cell culture results at high static fields and rapidly changing fields associated with the application of field gradients. Of the reported and measured effects in human subjects (e.g., vertigo, nystagmus, temperature elevations from absorbed RF power, and peripheral nerve stimulation), none has been limiting or considered harmful at allowed limits to 9.4 T (Kangarlu et al., 1999; Chakeres et al., 2003; Vaughan et al., 2006; Atkinson et al., 2007, 2010a). U.S. FDA investigational device exemption (IDE) has been approved to 9.4 T, and evaluation of the new threshold of 10.5 T began in 2015 at the University of Minnesota.

Animal studies to 21.1 T have not revealed any physiological or health problems beyond those known for brief exposures; however, many effects scale with body size (e.g., conductive loop diameters, vessel diameter, flow speeds). Eleven mechanisms leading to physiological effects are summarized below. Of these, six require further investigations through experimental studies in order to verify no irreversible physiological effects at 14–20 T. A quantitative evaluation given here for high-field exposures leads to less concerns regarding hazards from susceptibility anisotropy and implanted ferromagnetic objects. Induced current densities from high amplitude gradients and switching rates higher than current practices remain concerns, but these pertain to MRI and MRS at contemporary as well as very high fields. Information is presented on the potential importance of free radical (reactive oxygen and nitrogen species) lifetime prolongations associated with both low- and high-amplitude magnetic field exposures. Many effects including effects on molecules and molecular assemblages are rapidly reversed as long as exposures are not over periods longer than MRI and MRS magnetic field exposures of a few hours. The 11 topics discussed in this section are listed below. Topics that require large animal experimentation or more investigation are flagged (*).

*RF Power Deposition**

*Acoustic noise from gradients **

Ferromagnetic implants and projectiles

Diamagnetic Forces (volume forces)

Lorentz forces on ionic currents

Vestibular Organ Effects

Lateral forces on nerve axons

*Induced electric potentials from fluid flow—Faraday law **

*Magneto-hydrodynamic retarding force on flowing blood **

*Induced E-fields on nerves and brain from time varying gradients**

*Magnetic field effects on molecules, tissues and cells **

RF power deposition, Specific Absorbed Power (SAR)

The oscillating magnetic fields for the radiofrequency pulses used in imaging and spectroscopy induce oscillating electric fields in accord with Faraday induction as already discussed relative to time varying gradients. The E field is proportional to the frequency and the conducting body loop. The average electric field induced by the changing magnetic field of the radiofrequency pulses is $E/\sqrt{2}$, and the specific absorbed power ratio, SAR, to a mass of tissue is:

$$SAR = |E|^2 \sigma / 2\rho \quad (2)$$

where $|E|$ is the magnitude of the E-field, σ is the conductivity, and ρ is the density.

Increase in field leads to increase in the magnetic resonance frequency for a given NMR nucleus with spin. In turn the increase in frequency leads to an increase in induced E-field thus the SAR is expected to increase with field. The increase in conductivity by a factor of 1.5 between 300 MHz (7 T) and 852 MHz (20 T). is a minor component of the expected increase in deposition of power

The principal concerns are prohibitive RF power (i.e., rate of energy deposition in tissues, SAR) and RF penetration limitations (i.e., frequency dependent absorption) at much higher proton frequencies

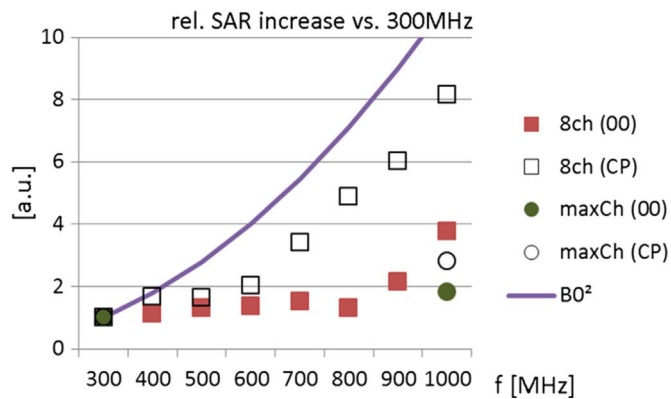


Fig. 11. Specific absorbed power (SAR) vs. frequency for 8 channel and maximum number of antenna arrays driven in circular polarized (CP) mode and in-phase (OO) with 0° phase shift between transmit elements. (From Winter and Niendorf, 2016, with permission).

than currently associated with available fields (i.e., 10.5 T and 11.7 T). But these can be mitigated by the advances in RF coil designs. In contradiction to the traditionally cited quadratic dependency espoused by many over the last 30 years (e.g., Röschmann, 1987), simulations using multipole-expansions followed by verification experiments with surface coils showed a flattening of the SAR vs. magnetic field beyond 430 MHz (Keltner et al., 1991). That work was verified using similar electrodynamic principles by Lattanzi and co-workers (2009) who reported that the ultimate intrinsic SAR shows a flattening or slight reduction with increasing field strength and by Winter and Niendorf (2016) multiple dipole array head coil simulations (Fig. 11).

For lower gamma nuclei such as O-17, Na-23, Cl-35, and K-39, the resonance frequencies up to those required for 20 T are below 300 MHz (Table 3) and MRI/MRS studies of these nuclei do not have the SAR problem of high frequencies but do have limitations due to their lower sensitivity and short relaxation times. Special RF sequences used for these nuclei in the multiple quantum studies also challenge the current power deposition limits. A particular focus in developing pulse sequences and RF coils will be to keep the SAR within allowable limits.

Acoustic noise

Acoustic noise associated with vibrations of the gradient coil due to Lorentz forces is of a magnitude that patients, particularly small children and mentally ill subjects, are made uncomfortable, and the sound power level (SPL) can lead to changes in brain function images at almost all magnetic fields being used (Bandettini et al., 1998). The loudness and frequency characteristics of this noise are dependent on the main field strength, pulse sequence, gradient coil construction and environment (Cho et al., 1997; Hattori et al., 2007). U.S. FDA guidelines stipulate a maximum peak limit at 140 dB and an average level with ear plugs of 99 dB.

The increase in sound level with the B_0 field does not appear to be linear based on early measurements that showed ramping from 0.5 to 1.0 T and from 1.0 to 2.0 T resulted in an SPL increase of 5.7 and 5.2 dB(L), respectively, when averaged over the various pulse sequences (Moelker et al., 2003). Based on logarithmic scaling of $20 \log(\Delta B_0)$ one can predict an increase of 6 dB for a field doubling. In the case of going from 7 T to 20 T the expectation based on a logarithmic increase would be a SPL increase of 9 dB. But the increase might be substantially less based on theoretical computer stimulations of vibroacoustic noise that compared SPL for B_0 fields of 3 T, 7 T and 10.5 T. The spectrally averaged SPLs were 91.2, 97.5, and 100.8 dB if Lorentz dampening is not included, and 92.1, 89.8, 90.5 dB when Lorentz damping is included in the simulations (Winkler et al., 2015).

Methods proposed to reduce sound noise include an antiphase noise-cancellation technique (Goldman et al., 1989), a Lorentz force-

cancellation technique (Mansfield et al., 1995), specialized pulse sequences (Costagli et al., 2015) and the use of ear plugs. None of these methods has been entirely satisfactory, as they do not mitigate sound transmission to the auditory system either directly or indirectly through the body structures.

Gradient coil construction using computer-aided design (Rausch et al., 2005) as well as the design of pulse sequences can aid in mitigating the acoustic levels as systems reach higher gradients and higher magnetic fields. Development of 20 T human MRI will require consideration of all the sources of the noise in the system design (i.e., electromechanical interactions between gradient coils, dc coils, the cryostat, and other system components) as well as system operation (specialized pulse sequences, etc.). Cryostat design principles used in large magnet systems to minimize forces during quench might contribute to acoustic noise mitigation (Chen et al., 2010).

Another source of noise is from acute temperature rises and tissue expansion that cause a pressure pulse due to RF heating (Röschmann, 1991). This acoustic effect is masked by other noises and is not considered harmful.

Ferromagnetic implanted devices and projectiles

A first concern of very high magnetic fields is the danger from ferromagnetic materials including tools, metal furniture, and other ferromagnetic objects that can become projectiles. No unusual forces are expected for the higher-field magnets, as the ferromagnetic materials will have reached magnetization saturation already at 3 T. Extra caution to be taken at higher fields is based on the fringe field gradients, as the force on objects will be directly proportional to any increase in the fringe field gradient at a specific location. A related precaution is the hazard from movement of metallic implants including pacemakers, dental implants, orthopedic implants, aneurysm and hemostatic clips or other devices having ferromagnetic components. The hazards have been known since a report of an aneurysm clip dislodged during an MRI study (New et al., 1983). A short time after this incident an exhaustive investigation of specific materials commenced, leading to an annually updated compendium listing safe as well as hazardous materials (Shellock, 2016). The attractive forces will depend on the gradient on entering the magnet as ferromagnetic materials are saturated at fields beyond a few Tesla. It can be shown that the turning torque is independent of field strength (Nyenhuis et al., 2005). The current screening of individuals before entering the magnet is an adequate safeguard against harm arising from pacemakers and other implanted ferromagnetic objects.

A potential problem from dislodgement and movement of magnetic particles found in the human brain is considered here. These particles are similar to the magnetosomes seen in bacteria. The particles are single crystals of about 50 nm diameter or clusters of many crystals in the human brain (meninges) with concentrations estimated at 50 ppb (Kirschvink et al., 1992). Will magnetite particles at 50 ppb concentrations in parts of the human brain migrate as a function of exposure time duration to high fields and field gradients in proposed MRI systems of the future? As indicated above, forces on ferromagnetic objects including magnetite depend on the product of saturation magnetization and the spatial gradient. The maximum force is on entry into the magnet. The saturation magnetization of magnetite occurs at a magnetic flux density of about 1.2 T and reaches a value of only 0.025 T. But in a gradient of 4 T/m the force is 2 times that of gravity. It is not likely this high a gradient will be experienced even in the fringe field of a 20 T MRI magnet. The brain tissue material properties that will restrain migration and the time duration of exposure are factors required for an accurate prediction of the potential for particle migration. Recall these particles are 50 nm in diameter. The governing relationship for the ratio of force on magnetite to that of gravity is:

$$F_m/F_g = M_s \times dB/dz / (\mu_0 \rho \times g) \quad (3)$$

where F_m/F_g is the ratio of forces, M_s is the saturation magnetization, μ_0 is the permeability of free space, ρ is magnetite density, $5.15 \times 10^3 \text{ kg/m}^3$, and g is the acceleration of gravity.

Volume forces on diamagnetic tissues

Volume force on diamagnetic tissue is the product of tissue susceptibility, the B field and the B field gradient.

$$F/V = (\chi/\mu_0) B_0 \times dB/dz, \quad (4)$$

Here χ is susceptibility (e.g., for tissue, -9.05×10^{-6}), μ_0 is magnetic permeability ($4 \pi \times 10^{-7} \text{ N/A}^2$), B_0 (N/Am) is the main field and dB/dz the spatial gradient. The fringe field of 7 T commercial magnets results in a force that is 2.5% of the body force of gravity. This force calculation assumes the field and field gradient product is $36 \text{ T}^2/\text{m}$ (Franz14 Schmitt, 2014).

One naturally asks, what is the $B_0 \times dB/dz$ product to levitate a human subject?. The product of B-field and B-gradient that equals the density of the human times the acceleration of gravity is the value that will levitate a human subject. A 75 kg male with normal lungs has a density of 1050 kg/m^3 , and gravity is 9.8 m/s^2 . Equating Eq. (4) to the product of density and gravity gives the product of B_0 and dB/dz as $1428 \text{ T}^2/\text{m}$. The successful levitation of a frog was realized in the bore of a 16.4 T magnet (Berry and Geim, 1997). The force in Newtons required for levitating a 75 kg person is 225 times greater than that for a frog.

During imaging there will be fluctuating forces on volume elements of the brain due to applied gradients. This phenomenon has been investigated theoretically and experimentally using a water phantom and human subjects in a 4 T MRI and gradients less than 10 mT/m (Tomasi and Wang, 2007; Wang et al., 2010). The induced forces were generally less than 10^{-9} N per voxel. Even for tissue components with large magnetic susceptibilities such as iron containing proteins, the forces will be negligible. Susceptibility difference in some regions of the brain and head can be over 10 times those throughout the brain. In another study at 4 T (Wang et al., 2010) using phase imaging information, the induced forces in some regions such as the eyes and the pons were much larger but not significant (e.g., 10^{-8} N per voxel); yet considering the sensitivity of pressure sensors, one might expect a perception of pressure on entering the fringe field of the proposed high-field magnets due to the differential forces associated with adjacent tissues having differences in susceptibility of a few ppb.

How do these results relate to physiologic phenomena during human exposures to the fringe fields on entry into a 20 T MRI solenoid? We have shown the volume force magnitudes are small percentages of the force of gravity, but we have not shown the change in force with position on entering the magnet. The likelihood of a pressure sensation while in the fringe field can be estimated by comparing the volume force on a 1.7 kg human head at the entrance of a 7 T magnet to the force of gravity. The force on the human head entering a 7 T MRI with a field and field gradient product of $36 \text{ T}^2/\text{m}$ is only 2.6% of the force of gravity. While this is a small effect, the sensed pressure appears to be within the limits of perception and could explain the “feeling of some pressure” reported by some subjects.

Differences in forces on adjacent tissues are dependent on the small differences in susceptibility including layers of the human cortex. Shear forces between tissue and fat or tissue and bone might be sensed but not be uncomfortable. But the susceptibility differences between iron-loaded tissues and adjacent tissues such as the cerebral cortex (Fukunaga et al., 2010) and other tissues (Schenck, 1996) will need evaluation as these will increase with field increases. A diamagnetic shear force will occur when adjacent tissues with different susceptibilities experience a gradient as on entering the magnet. In a static field the torque associated with susceptibility anisotropy will vary with

field squared as well as the direction of the field. For ferromagnetic objects such as aneurysm clips and pacemakers that have saturable magnetization, the torque is not field dependent (Nyenhuus et al., 2005).

Lorentz forces on ionic currents

Lorentz force on vestibular semi-circular canal receptors

The most commonly reported sensations experienced by subjects on entering as well as in a high static magnetic field instrument is vertigo (i.e., a dizzying or body tilting sensation or perception of spinning surroundings). The subject reports incidences were a few percent at 4 T and 30% at 7 T (Versluis et al., 2013). These sensations have been under investigation for the last 24 years (e.g., Schenck, 1992; Roberts et al., 2011; Patel et al., 2008; Antunes et al., 2012; Mian et al., 2016). This phenomenon is a magnetic field effect on the vestibular apparatus. The vestibular apparatus is shown to be involved because the effects of turning and head tilt in rodents (Houpt et al., 2011) disappear after excision of the vestibular apparatus (Cason et al., 2009).

The vestibular organ (Fig. 12) has two major functions: sensing sound and sensing position and change of position relative to gravity. This complex organ detects sound by vibrations that enter the spiral portion known as the cochlea. Extremely sensitive hair cells that line the cochlea canals send signals to the brain when sound pressures are transmitted from vibrations of the ear drum. The circular structures orthogonal to one another and the remaining structures of the vestibular apparatus are sensors for the direction of gravity, linear motion and angular motion. Gravity and linear accelerations are detected by the distortion of a gel-like structure having embedded little stones (calcium carbonate). This matrix motion is detected by the distortion of multiple hair cells. Angular motion is sensed by the differential inertial motion of lymph in the semicircular canals relative to the semicircular canals that are oriented in three directions as shown by the model. Fluid motion in the semicircular loops or canals will lag the motion of the head, and this shear force will excite the hair cells in the cupula sensor at the base of the semicircular canals. The signals that are integrated with information from the visual system and body position sensors (proprioceptors) facilitate body balance. But if the body pressure sensors and visual clues regarding position are in conflict with information from the gravity and motion sensors, dizziness or vertigo occurs.

The mechanism for the sensation of dizziness, nausea and signs such as nystagmus in a static magnetic field is now generally accepted as the result of Lorentz forces wherein the magnetic field interacts with permanent ionic currents of the endolymph fluid of the semicircular canals (Roberts et al., 2011; Antunes et al., 2012; Mian et al., 2016). If the canal is oriented appropriately with respect to the magnetic field, the force of the conductive fluid will put pressure on the hair cells of the cupula. This constant force will lead to vertigo, but as with many physical effects leading to conflicts with sensors, the body will compensate and thus the sensations are only temporary. But head motion will lead to a new direction of force on the hair cells of one or more of the semicircular canals and thus another episode of temporary vertigo. The modeling and experimental work of Roberts et al. (2011) led to the conclusion that the force per cupula area was between 0.02 and 0.002 Pa. These are greater than the nystagmus threshold of 0.0002 Pa (Oman and Young, 1972).

The expected cupula stimulation pressure on exposure to 20 T can be calculated based on the endolymph current of $J = 70 \text{ nA}$ used by Roberts et al. (2011), an assumption of the space above the cupula of $d = 1 \text{ mm}$, and a cupula area of $A = 0.01 \text{ cm}^2$ (Oman and Young, 1972). The Lorentz force divided by area ($d \times J \times B/A$) is 0.0014 P. The parameters for this calculation are estimates only, yet the forces are within reason and are not of concern.

Another mechanism for stimulation of the vestibular apparatus is

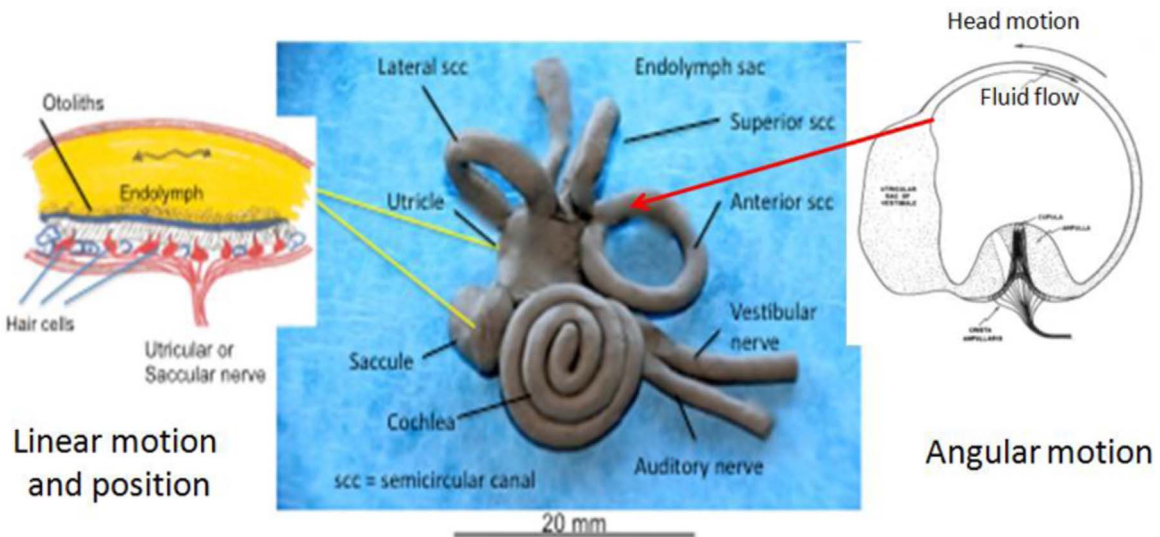


Fig. 12. The vestibular organ occupies the bony labyrinth and has three major parts and functions: the cochlea (spiral structure) for hearing, the semicircular canals for sensing rotational accelerations and the utricle and sacula responsible for sensing position relative to gravity and linear acceleration. The differential motion between head motion and the endolymph in the semicircular canals is detected by deflection of tiny hairs of the hair cells on the cupula in the fluid filled canals. Position and linear motion are sensed by deflections of similar hair cells caused by the motion of small particles called otoliths in the sacula and utricle.

induction of current densities through rapid changes in magnetic fields associated with MRI imaging gradients. This mechanism for stimulation of peripheral nerves and visual sensations is discussed below but mentioned here, as it could account for sensations by subjects exposed to rapidly switched, high-amplitude gradients and should be included in considerations of causes for sensations of vertigo, nystagmus, nausea and sensations of body discomfort. Noteworthy is the fact that rodents that demonstrate avoidance behavior when entering a high magnetic field require an intact vestibular system (Haupt et al., 2007).

Lorentz force on nerve axons at 20 T

The lateral force on a conducting neuron (current density about 9 A/m^2) will lead to some displacement proportional to the current and the field orthogonal to the current as expected from the Lorentz current-field relationship. The amount of deviation that can be expected at 20 T is calculated using the derivation of Roth and Bassler (2009) used for lower fields. The lateral displacement is $64 \text{ }\mu\text{m}$. Though this magnitude is less than would be realized in MRI images and is not expected to have physiological consequences, it can lead to artifacts in very high resolution images approaching $100 \text{ }\mu\text{m}$ resolution as well as artifacts in vision during exposures.

Nerve impulse conduction speed effects

Sodium, potassium, chloride, and calcium ions migrate in the extracellular space during nerve conduction, and their paths can be distorted or impeded during nerve impulse propagation in a magnetic field by two mechanisms. One is through distortions of the ion current paths by the Lorentz force associated with a field perpendicular to some extent to the ion current direction, and the other is by a change in the hydrated state of electrolyte ions. The first effect was analyzed theoretically by Wikswo and Barach (1980) who estimated a 10% slowing at 24 T for a magnetic field at right angles to the conduction direction. Their model is a myelinated nerve consisting of gaps (nodes of Ranvier) between the covering Schwann cell insulation. The propagation is facilitated by extracellular ion loops intersecting the neuron every $100 \text{ }\mu\text{m}$ at the nodes of Ranvier. The myelinated nerve conduction speed is about 12 m/s and varies with nerve diameter. Ion drift speed estimates vary over orders of magnitude, and the speeds used in this prediction were not given. The importance of this effect can be investigated using standard nerve conduction speed experiments in high magnetic field facilities with care to control temperature as nerve

conduction is very sensitive to temperature variations (e.g., 1% change with $0.1 \text{ }^\circ\text{C}$ change).

The effect on electrolyte hydration proposed here for investigation is inferred from measurements of viscosity changes at fields below 0.3 T (Cai et al., 2009). This effect on nerve conduction speed has not been evaluated, and no measurements of the magnetic field effects on electrolyte viscosity have been found for fields higher than 0.3 T . Magnetic field effects on viscosity and nerve conduction speed can be evaluated using conventional nerve in vitro preparations and static high magnetic fields.

Induced electric potentials and the magnetohydrodynamic force

Faraday effect from blood flow

Blood is an ionic conductor, and its flux in a magnetic field will result in an induced voltage, which is proportional to the flow (current) and the diameter of the vessel (e.g., the aorta) if the flow is orthogonal to the magnetic field:

$$V = v B d. \quad (5)$$

For the human aorta, a flow $v = 1 \text{ m/s}$ in a field of 20 T and diameter of 0.016 m gives the emf as 0.32 V . No problems with cardiac rhythm have been noted in human exposures of many subjects to 9.4 T (Atkinson et al., 2007, 2010a). Tenforde (2005) predicted on theoretical grounds a current density near the sinoatrial node of the heart of 220 mA/m^2 on the assumption that significant leakage currents occur, but the aorta specific resistance is 6 orders of magnitude larger than the specific resistance of blood; thus, the predicted current densities cannot occur. Based on data from (Watson et al., 1973), the current density to fibrillate the human heart is 3000 mA/m^2 ($300 \text{ }\mu\text{A/cm}^2$). The evaluation of untoward electrical phenomena requires detailed modeling using high-fidelity spatial specific resistivity maps but there are no experimental data that suggest the induced voltages from blood flow will become a problem at 20 T . A multitude of canine studies have been completed at 11.1 T with no cardiac events observed (Univ. of Florida, Gainesville). The induced voltages and resultant current densities from blood flow in large vessels will increase linearly with field increase. But there are no concerns for the human brain magnet as the effect scales with vascular diameter and large vessels will not be in the high magnetic field.

Magneto-hydrodynamic blood flow retardation

Magneto-hydrodynamic (MHD) force refers to the modification of conductive fluid or charged particle plasma flow by the presence of a magnetic field. It is sometimes used to describe the voltage generated by a conductive fluid in a magnetic field, but that is not the complete magneto-hydrodynamic effect of a force opposing the flow of a conducting fluid in an orthogonally directed magnetic field. The E-field generated by movement of a conductive medium in a magnetic field will itself interact with the magnetic field, which will produce an increase in blood pressure downstream to maintain adequate tissue oxygenation. With high enough conductivity (e.g., mercury) and magnetic field, the retarding pressure can stop flow. Literature prior to 1990 suggested that this effect could lead to important blood pressure elevations at fields beyond 15 T. Experiments in 1990 (Keltner et al., 1990) showed the simulations done previously were incorrect, and a new theoretical simulation that included more complete physics showed only a 0.2% pressure increase at 10 T. Thus, simulations and experimental verification need to include fields up to 20 T. The experimental work requires a high field magnet with a bore large enough to accommodate electrolyte flow in 20 mm diameter tubes orthogonal to the field direction in a phantom such as shown in Fig. 13. But noteworthy is the fact that almost all of the large blood-flow vessels in the body will not be affected by this effect as they are parallel to the B field and the carotid and vertebral vessels have 1/4th the diameter of the aorta.

Peripheral nerve stimulation from time varying gradients

A now well-known issue for MRI at all fields is peripheral nerve stimulation (PNS) by the gradients used for imaging as well as gradients used in selective region spectroscopy. In addition to peripheral nerve/muscular stimulation, rapid changes in magnetic fields stimulate sensations of light flashes and can in theory stimulate the vestibular apparatus as a result of induced current densities from changes in magnetic field near the human head. The physiology of nerve and neuromotor stimulation related to induced E-fields and possibly induced turning torques on macromolecular assemblages with susceptibility anisotropy (e.g. retinal rods) continues to be a subject that requires more investigation as thresholds for stimulation depend on more parameters than a simple calculation of induced E-fields and related current densities. The following sections discuss neuronal stimulation from rapidly changing magnetic fields on the body, vestibular apparatus, brain and visual system.

The induction of the E-field from a time-varying magnetic field and the sensation experienced by exposed subjects is explained as follows. An E-field of 6 V/m induced by 60 T/s near a 30 cm diameter conducting body will cause sensations of an electric shock, sensation

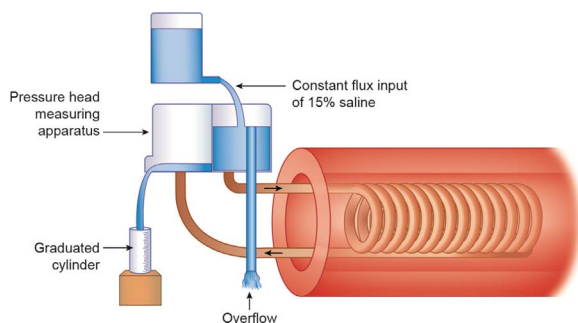


Fig. 13. Experiment to measure the magneto-hydrodynamic retarding forces at 2.35 T and 4.7 T with flows using 15% saline up to 7 l per minute. These experiments verified the theoretical predictions that showed no significant effects at these fields. The theoretical prediction for blood flow at 10 T is a 0.2% increase in pressure. This apparatus is appropriate for experimental measurements of retarding forces in very high field, large bore, non-MRI magnets available at fields of 20 T and beyond. (From Budinger et al., 2016, with permission).

of tightening of the thorax or a dull pressure sensation. The sensation that is usually reported at the threshold of the effect is a slight electric shock. The governing physics is the Maxwell-Faraday equation that equates the electric field to the diameter and conductivity of the tissues' circular conductor loops orthogonal to the direction of the magnetic field as well as the rate of change of the magnetic field, the waveform (McIntyre and Grill, 2002) and the frequency. The governing equation for the E-field (V/m) as shown here does not include the factors of waveform and pulse train frequency:)

$$V/m = -dB/dt \times r/2, \quad (6)$$

where dB/dt is the rate of the magnetic field change and r is the object radius seen by the inductor. Note that a change in the area of a conductor (dA/dt) in a constant B field will also induce an E-field; thus, chest expansion and cardiac chamber size changes will result in a voltage potential superposed on the standard electrocardiogram recording in addition to the superposed voltage from cardiac blood flow (e.g., about 1 mV) across the ECG chest leads. The current density associated with the induced E-field is

$$J = dB/dt \sigma r/2, \quad (7)$$

where σ is the conductivity. The current density for a current loop of radius $r = 10$ cm, $\sigma = 0.2$ Siemen/m and dB/dt of 1 T/s is $1 \mu\text{A}/\text{cm}^2$. Estimates of nerve stimulation and evaluation of thresholds for nerve, muscle, heart, brain and visual phenomena cannot be made based simply on these equations, as the mechanism of the stimulus effect depends on rise time, pulse shape, frequency, number of pulses per pulse train as well as the current paths in the body (Budinger et al., 1991; Irnich and Schmitt, 1995; Reilly 1998). The E-field distributions are dependent on the gradient coil design and these E-fields as well as the resultant current densities can be evaluated through computation simulations and knowledge of tissue conductivity distributions (Nyenhuys et al., 1997).

The early experiments to determine thresholds in human subjects are shown as a function of number of pulses, frequency and peak B-field in Fig. 14 (Budinger et al., 1991). Similar results were shown in corroborating studies (Mansfield and Harvey 1993). These data fit what has been known by the electrophysiologists as the "fundamental law of electrostimulation." The defining function is a hyperbolic curve also known as an "intensity-duration curve," which will have a shape similar to the curves of Fig. 14. Details of the relevant parameters that define this intensity-duration curve are given by Irnich and Schnitt (1995). The importance of this electrophysiology is that it will define the engineering and related pulse sequences needed for improved MRI studies independent of field. But as field strength

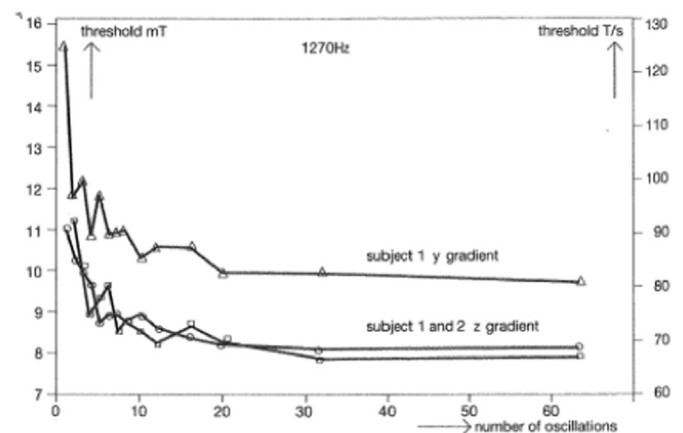


Fig. 14. Peripheral nerve stimulation from induced E-fields associated with MRI magnetic gradients. The threshold for a faint sensation of electric shock is a function of the number of pulses, and rate of field change for non-trapezoidal asymmetric wave forms similar to those of Fig. 15. (From Budinger et al. 1991, with permission).

allows higher sensitivity, the advantages for dMRI require higher gradient coil performances and thus the potential for brain and head tissue stimulation.

The threshold for generation of visual sensations (phosphenes), as distinguished from peripheral nerve stimulation sensations, is less than 2 T/s and unlikely to be due to an induced current density as discussed further below. These considerations are important as many opportunities at increased field strength depend on use of gradient coils that can generate gradients higher than 100 mT/m and switching times shorter than currently being used. Visual phosphenes should not be used to guide head gradient coil design (vide infra).

Electrical stimulation of the vestibular apparatus

Almost 200 years ago the physiologist Purkinje reported that electric (galvanic) currents flowing through the head caused loss of balance and equilibrium in test subjects, and by 1875 the vestibular organ was identified as the mediator (Breuer, 1875). The use of electric stimulation for electrophysiology has evolved over the last century (Fitzpatrick and Day, 2004), but details that enable current density threshold calculations cannot be found. This is important in order to determine whether the current densities are similar to those induced by contemporary switched gradients. The currents applied to 3-cm diameter electrodes with low-resistance coupling to the skin over the mastoid processes behind each ear are in the range of 0.1–0.3 mA. Though one can estimate a current density of $40 \mu\text{A}/\text{cm}^2$, this is not reliable, as the current paths between the electrodes are complex. The vestibular apparatus is not involved because galvanic stimuli are still effective in eliciting responses in subjects with no vestibular apparatus but an intact eighth cranial nerve. The time interval from stimulus to motor response is 120 ms, which implies a conduction velocity of 8 m/s from the head to thorax and leg peripheral muscles that are responsible for postural control. This rapid response of posture change suggests that the electrical stimulus must be independent of brain processing. Work by others at much higher currents evokes a response to the periphery within 60 ms. These facts point toward a direct eighth nerve stimulus and the need for a broader investigation of the effects of E-field inductions by gradient amplitudes, waveforms and slew rates.

Electrical stimulation of the brain

Though the magnitude of the static field does not affect the induced current densities from gradient coils being proposed at both contemporary and higher magnetic field applications, many of the proposed high field applications in neuroscience are dependent on high gradients and high gradient slew rates. Brain stimulation thresholds are not expected to be the same as peripheral nerve stimulation thresholds, thus for guidance we turn to what is known from repetitive transcranial magnetic stimulation (rTMS) and transcranial direct current stimulation (tDCS) used in clinical programs. Safety aspects of rTMS and tDCS have been reviewed recently (Rossi et al., 2009).

The method of direct current stimulation using non-depolarizing currents employs 3 cm^2 electrodes placed in different positions over the skull with a reference electrode on the head or periphery. A review of 95 experiments collected for a 10 year period by an international group summarized the multitude of effects ranging from brain blood flow changes measured by PET and fMRI to cognitive and mood changes (Nitsche et al., 2008). The current densities were mostly between 29 and $57 \mu\text{A}/\text{cm}^2$. Peripheral sensations were not reported beyond electrode tingling. The importance of these observations, considered safe and even therapeutic in some cases (e.g., depression), is that the MRI/MRS gradients being proposed will generate current densities in a similar range. But thresholds for short and long-term effects are unknown currently.

Relevant to induced E-fields from gradient coils are the experiences from thousands of patients undergoing transcranial magnetic stimulations (rTMS) for the treatment of a variety of diseases. Success of these methods led to approval for some conditions by the Food and Drug

Administration in the USA. The stimulators and coils currently in production develop about 1.5–2.0 T (T) at the face of the coil and produce currents changing at rates up to $170 \text{ A}/\mu\text{s}$ (Thielscher and Kammer, 2002). The cortex E-fields are as high as 150 V/m. These induced E-fields go beyond the threshold for stimulation of peripheral neuromotor systems. These stimulators are able to activate cortical neurons at a depth of 1.5–3.0 cm beneath the scalp using standard, "figure 8", circular or double-cone coils. The electric field distributions for TMS coils have been evaluated (Roth et al., 2007). The opportunities for optimization of coil designs to deliver higher performance by avoiding stimulation of peripheral nerves of the head will require more investigations as use of the derived current densities used in direct electrical stimulation for surface electrodes cannot be directly related to current densities from induced E-fields. The current standards promulgated by the International Technological Commission (2015) specify gradient waveforms and slew rates, but these guidelines or standards might not be applicable to contemporary gradient coils needed for human neuroscience investigations. The investigations of optimum head gradient coil designs are independent of the static field except for Lorentz force mechanical considerations.

Visual sensations from time varying gradient fields

Visual sensations such as perception of light associated with a changing magnetic flux density near the human head are known as phosphenes (sensations of light). Phosphenes are also induced by electric currents and a pressure tap to the side of the eyeball. Other causes of light sensations are galactic cosmic particles (accelerated heavy ions) and gamma radiation in the 10 s of keV range in the dark adapted eye (Tobias et al., 1971, Budinger et al., 1972). Magnetophosphenes can be induced at about 2 T/s and have a peak B-field threshold and a frequency response unlike that for peripheral nerve stimulation. This phenomenon has been studied since visual phosphenes were noted in 1896 by d'Arsonval (d'Arsonval, 1896), who moved a magnetic field source near the eyes. The history of visual phosphene developments using electricity and magnets (Marg, 1991) and ionizing radiation gives evidence that visual sensations can be elicited by a number of causes such as induced E-fields, shear stress from retinal rod susceptibility anisotropy, or sound pressures; thus, cannot be relied upon for determining thresholds for gradient coil designs. The threshold for visual sensations is dependent on reaching a field of at least 10 mT with a rise time of approximately 2 ms and a repetition rate less than 40 per second (Budinger et al., 1984). These parameters were determined experimentally in a 30-cm diameter solenoid with a wave form shown in Fig. 15. The flickering observed

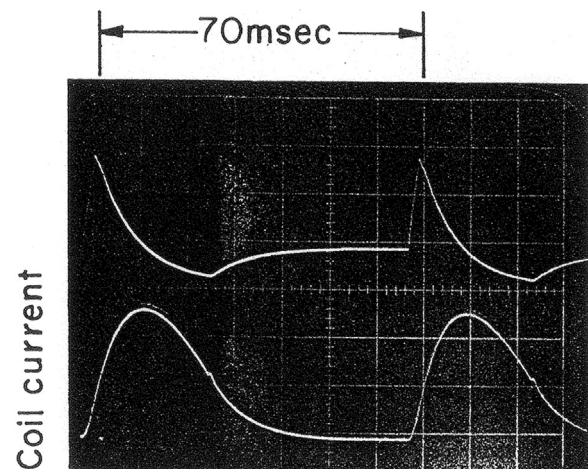


Fig. 15. Stimulation of visual phenomena (phosphenes) has a much lower current density threshold than that for peripheral nerve stimulation. Shown is the magnetic field waveform (upper) and coil current (lower) energized by a water cooled 52-turn solenoid 30 cm wide and 37 cm long for human head insertion.

by five subjects is not dependent on dark adaptation. Visual phenomena could not be produced in experiments using 210 T/s with pulses of 3 μ s duration. The minimum threshold at about 30 Hz corresponds to observations by others (Lövsund et al., 1980). Though neuroscientists and imaging scientists believe magnetophosphenes are caused by induced electrical currents, an alternative explanation is that the phenomenon is the result of diamagnetic forces on retinal rods as a result of susceptibility anisotropy. Direct electric voltage application to the head can induce phosphenes, but the current densities of 17 μ A/cm² (Barlow et al., 1947) are much greater than 2 μ A/cm² that are calculated from magnetic field change experiments (Fig. 15). The emphasis on the mechanisms for phosphene observations is relevant to understanding other sensory phenomena that might manifest at 20 T where larger fringe fields and B fields are expected than have been experienced in the last 35 years of investigations.

Magnetic field effects on molecules, tissues and cells

In the sections above the physics and physiology of static magnetic fields, switched gradient fields and RF interactions with biological tissues were reviewed with respect to effects anticipated up to 20 T magnetic field exposures. The purpose of this section is to briefly review the current state of knowledge regarding the genotoxic and carcinogenic potentials for ultrahigh magnetic field MRI. Starting 35 years ago possible harmful effects of MRI came under investigation (Budinger, 1979; Wolff et al., 1980). The experiments include molecular, subcellular, cellular and tissue effects of static and oscillating magnetic fields. More recently there have been extensive reviews of effects of static magnetic fields ranging from 50 μ T to 15 T on chemical and biologic systems (Okano, 2008) and effects of static low-frequency and pulsed magnetic fields (Ueno and Okano, 2012). The extensive summary of static and time-varying field effects showed as many positive as negative results and this is the case for other studies (e.g., Schenck, 2005; Vijayalaxmi and Speck, 2015; Foster et al., 2017).

Non-controversial effects at the macromolecular level are magnetic orientation or torque phenomena observed for large molecular assemblages in vitro such as chloroplasts and retinal rods. These effects are based on magnetic anisotropy (Hong, 1995; Schenck, 1996). The magnetic energy associated with the orientation changes of molecular assemblages is proportional to the magnetic field squared as is the rate of orientation change. Retinal rods in a petri dish are oriented by 90° in less than 10 s. In tissue no movement occurs due to the overwhelming restraining adhesive forces. Biophysical consequences of in vitro exposures to high static fields have been reported. Examples are structural changes in tubulin (Bras et al., 1998), alterations of the cleavage plane in developing frog eggs (Denegre et al., 1998) and abnormalities in fibroblast and neuronal growth at fields up to 15 T (Valiron et al., 2005). Mechanisms that can account for these observations include chemical separations, effects on hydrated states of ions such as drift velocities (Cai et al., 2009), and prolongation of the life times of oxygen and nitrogen free radicals arising from naturally occurring chemical transformations discussed below. But these mechanisms have yet to be verified. No deleterious observations have been reported from extensive studies on rodents at 21.1 T by NHMFL investigators other than temporary effects on the vestibular apparatus (vide supra).

In the past few years possible effects on DNA such as double-strand breaks (DSB) have been reported in blood samples (leukocytes) from subjects undergoing cardiac MRI protocols with and without injected contrast material. There are as many positive as negative reports for evidence of some short-term effects on lymphocytes from subjects exposed to fields up to 7 T (e.g., Vijayalaxmi and Speck, 2015; Fatahi et al., 2016). What are missing from some of these experiments are proper positive controls and analyses of confounding variables (Foster et al., 2017). Known causes of DNA DSB include UV, ionizing radiation (X-ray CT), virus infections and environmental temperature

(Giovannelli et al., 2006) as well as beta blockers used by cardiovascular patients and MRI contrast agents. Reports of DSB findings are in a background of 50 DSB per cell per cell cycle almost all of which are immediately repaired (Vilenchik and Knudson, 2003) leaving experimentally visualized foci of breaks at the level of about 0.11 DSB per cell.

Free radical effects of static and time varying magnetic fields

It is well known in physical chemistry that static or oscillating magnetic fields can influence the kinetics and life times or yields of free radicals. The underlying reaction scheme is well-known for over 25 years and is described by the radical pair mechanism (Steiner and Ulrich, 1989). This mechanism has been proposed as a plausible explanation for presumed health effects from environmental electromagnetic fields with frequencies of 50–60 Hz, radio frequencies and cell phone exposures. The arguments against non-ionizing fields as causative of health effects is that the photon energies are about 100,000 times smaller than single bond energies, but bond breakage is not the mechanism involved in the reaction kinetics of free radicals. Free radicals are chemical molecules or atoms with an electron that does not have a partner with an opposite spin. They are intermediaries in biochemical reactions and are essential for many enzyme systems. In tissues, free radicals combine with one another, or with single atoms that also carry free electrons. This results in ordinary molecules, all of whose electrons are paired; or free radical molecules react with intact molecules, to extract parts of the molecules to complete their own electron pairs thus generating new free radicals in the process.

The major free radical of the human body is superoxide (an oxygen molecule with an extra electron). Superoxide molecules are needed as part of the body's oxidation and reduction biochemistry. They are a by-product of cellular energy production, and an essential part of the immune system. Superoxide is necessary for sustaining health but an over abundance causes cellular injury including DNA damage. The controlling enzyme is superoxide dismutase which converts superoxide to hydrogen peroxide, which in turn is modulated by the enzyme catalase to produce hydrogen and water. Dysfunction of either of these enzymes or an increase in concentration or life-times of superoxide molecules can result in macromolecule and tissue injuries. Superoxide excess can be stimulated by toxins, mitogens, heat, ultraviolet or high-intensity laser photons, and ionizing radiation. For example Con A, a mitogen, that induces Ca⁺⁺ uptake in rat thymic lymphocytes has been shown to depend on the generation of reactive oxygen radical species (Gukovskaya et al., 1989).

An external magnetic field influences radical pairs generally by slowing down processes that require a change in spin. In the presence of a magnetic field less radicals can change their spin and more succeed in separating from their partner. The consequence is that the free radical concentration increases when a magnetic field is applied (Scaiano, 1995). Static magnetic fields can affect singlet–triplet transitions in unpaired electrons and the increased lifetime of free radicals, which can directly or indirectly damage neighboring biomolecules such as DNA, proteins, and membrane lipids (Wiseman and Halliwell, 1996). Biological effects depend on some level of spatial confinement of the free radicals, the initial production or concentration of free radicals, and the efficiency of the natural free radical scavenging system.

The radical-pair mechanism provides one explanation of magnetic field effects in biological systems. But the multitude of experiments in cell cultures, animals and human subjects have not given consistent results except those that include a co-stimulant such as a combination of ionizing radiation and magnetic field exposure, or the use of a chemical stress that is known to increase the free radical concentration. To explore this in the past we used radioactive ⁴⁵Ca to detect any effects of low-frequency magnetic fields on calcium flux into lymphocytes with and without a co-stimulant, the mitogen Con-A (Walleczek and Budinger, 1992). Magnetic field exposure used 3 Hz trapezoidal pulses

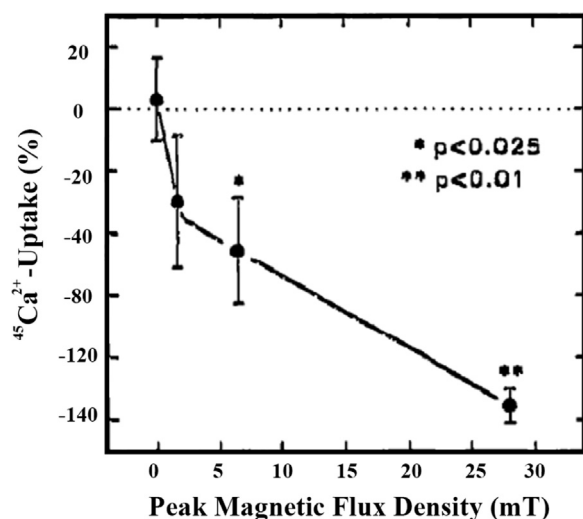


Fig. 16. Calcium ion uptake kinetics of thymus lymphocytes in a 3-Hz pulsed magnetic field in vitro. Bars are standard error of the mean. Cell stimulus is the mitogen Con-A. The number (n) of individual experiments at each peak magnetic flux density value is: 0 mT (n = 4), 1.6 mT (n=4), 6.5 mT (n=10) and 28.0 mT (n=3). (From Walleczek and Budinger (1992) with permission).

to 30 mT. There was a significant effect but only if the co-stimulant was present (Fig. 16). The possible mechanism for a magnetically-sensitive, radical-dependent processes that could influence mitogen-induced lymphocyte Ca^{++} signaling is that cytochrome P-450 activity may be involved in Ca^{++} uptake regulation in rat thymic lymphocytes (Alvarez et al., 1992) and that P-450 function proceeds via radical pair recombination steps (Hollenberg, 1992). Reviews of the involvement of magnetic fields with free radical mediated metabolic processes are found) for static fields (Ghodbane et al., 2013; Okano, 2008) and for environmental electromagnetic fields (Brocklehurst and McLauchlan, 1996).

Although animal studies to 21.1 T have not shown more than temporary physiological effects and there are no reports of harmful effects in human studies up to 9.4 T, effects of fields of 10 T and beyond on replicating cells or growing tissues will require investigations to discover mechanisms that are not associated with the unnatural biological environment of the magnet, sample preparations, and flawed statistics. In sum, whereas the mammalian systems have well known capabilities to adapt to short term physical stresses such as pressure, heat, ultraviolet fields, brief periods of anoxia, and stress related free radical generation, it is not known at what level and duration of exposure to magnetic fields the system will fail to adapt. Small animals including dogs and rabbits have been exposed to 11.1 T, 17.6 T and 21.1 T for more than one hour and there is no evidence of irreversible effects, short or long term.

Summary

Thirty-five years ago when MRI was recognized as an effective diagnostic method for clinical medicine, neuroscientists, and other medical scientists recognized that much more could be learned about the human brain from instruments with field strengths higher than 1.5 T. Thus by the 1990s, data from instruments that enabled human brain studies at 8 T and 9.4 T encouraged the development of instruments with a field as high as the then available superconducting material would allow at 11.7 T. During the past few years, new superconductor materials, cable configurations and solenoid coil configurations have been developed that make brain imaging and spectroscopy at fields of 14–20 T technically feasible.

Ten neuroscience goals achievable by higher magnetic fields than available currently are presented to justify the engineering develop-

ment effort and costs. Among the major neurological investigations enabled by higher fields are the detection of chemical and neural architectural correlates of human behavior and the improved understanding of the long term consequences of brain neuropathologies associated with injury and aging.

The sensitivity (SNR) and contrast to noise benefits as reviewed in this paper are shown to be greater than predicted in the past, including major improvements in SNR for proton spectroscopy. The RF penetration limitations, B_1 field inhomogeneities, absorbed power (SAR) associated with high frequencies, head motion, and potential biophysical safety concerns are shown to be problems for which there are solutions through physics, applied mathematics and engineering innovations. This paper also investigates the biophysics and physiology with respect to MRI at 14 T to 20 T, with the conclusion that pending results of planned large animal exposures (e.g., magnetohydrodynamic and Lorentz force effects) MRI and MRS studies at the proposed fields will not have effects other than temporary vertigo.

Technology developments for increased gradient amplitudes and slew rates necessary to realize the full benefits of high static magnetic fields are on-going. Physiologic thresholds for induced E-fields on the brain, vestibular and visual systems are not the same as thresholds for peripheral neuromuscular systems; thus, more attention is needed for optimization of coils and pulse sequences in order to achieve the potentials of ultra high field MRI and MRS.

The magnet costs depend on the new developments in high-temperature superconductors (HTS), cryocooling engineering and potential need for operations in non-persistent mode. The initiative to achieve 14 T to 20 T MRI envisions the development of a center for all scientists interested in basic neuroscience research on the functions of the human brain. This technology is predicted to enable quantification of biochemical components of the functioning brain not detectable heretofore.

Conflict of interest

Neither author has a conflict-of-interest, nor any commercial involvement.

Copyright notice

This manuscript has been authored by an author at Lawrence Berkeley National Laboratory under Contract No. DE-AC02-05CH11231 with the U.S. Department of Energy. The U.S. Government retains, and the publisher, by accepting the article for publication, acknowledges, that the U.S. Government retains a non-exclusive, paid-up, irrevocable, world-wide license to publish or reproduce the published form of this manuscript, or allow others to do so, for U.S. Government purposes.

Disclaimer

This document was prepared as an account of work sponsored by the United States Government. While this document is believed to contain correct information, neither the United States Government nor any agency thereof, nor the Regents of the University of California, nor any of their employees, makes any warranty, express or implied, or assumes any legal responsibility for the accuracy, completeness, or usefulness of any information, apparatus, product, or process disclosed, or represents that its use would not infringe privately owned rights. Reference herein to any specific commercial product, process, or service by its trade name, trademark, manufacturer, or otherwise, does not necessarily constitute or imply its endorsement, recommendation, or favoring by the United States Government or any agency thereof, or the Regents of the University of California. The views and opinions of authors expressed herein do not necessarily state or reflect those of the United States Government or any agency thereof or the Regents of the University of California.

Acknowledgments

Helpful suggestions and data were supplied by Drs. David Feinberg, Lucio Frydman, Riccardo Lattanzi, Joanna Long, Thomas Mareci Thoralf Niendorf, Alexander Pines, William Rooney, Brian Rutt, John Schenck, Victor Schepkin, Dean Sherry, Daniel Sodickson, Charles Springer, Keith Thulborn, Kamil Uğurbil, Peter van Zijl and Lawrence Wald. Mr. Robert L. Smith assisted in collection of references and editing. This work was supported by the Director, Office of Science, Office of Basic Energy Sciences, of the U.S. Department of Energy under Contract No. DE-AC02-05CH11231, and the State of Florida.

References

- Alvarez, J., Montero, M., Garcia-Sancho, J., 1992. Cytochrome P450 may regulate plasma membrane Ca²⁺ permeability according to the filling state of the intracellular Ca²⁺ stores. *FASEB J* 6 (2), 786–792.
- Antunes, A., Glover, P.M., Li, Y., Mian, O.S., Day, B.L., 2012. Magnetic field effects on the vestibular system: calculation of the pressure on the cupula due to ionic current-induced Lorentz force. *Phys. Med. Biol.* 57, 4477–4487. (PubMed: 22722424).
- Atkinson, I.C., Thulborn, K.R., 2010b. Feasibility of mapping the tissue mass corrected bioscale of cerebral metabolic rate of oxygen consumption using 17-oxygen and 23-sodium MR imaging in a human brain at 9.4 T. *Neuroimage* 51, 723–733. (PubMed: 20188194).
- Atkinson, I.C., Renteria, L., Burd, H., Pliskin, N.H., Thulborn, K.R., 2007. Safety of human MRI at static fields above the FDA 8 T guideline: sodium imaging at 9.4 T does not affect vital signs or cognitive ability. *J. Magn. Reson. Imaging* 26, 1222–1227. (PubMed: 17969172).
- Atkinson, I.C., Sonstegaard, R., Pliskin, N.H., Thulborn, K.R., 2010a. Vital signs and cognitive function are not affected by 23-sodium and 17-oxygen magnetic resonance imaging of the human brain at 9.4 T. *J. Magn. Reson. Imaging* 32, 82–87. (PubMed: 20578014).
- Atkinson, I.C., Claiborne, T.C., Thulborn, K.R., 2014. Feasibility of 39-potassium MR imaging of a human brain at 9.4 T. *Magn. Reson. Med.* 71, 1819–1825. (PubMed: 23798343).
- Bandettini, P.A., Jesmanowicz, A., Van Kylen, J., Birn, R.M., Hyde, J.S., 1998. Functional MRI of brain activation induced by scanner acoustic noise. *Magn. Reson. Med.* 39 (3), 410–416.
- Barch, D.M.I., Burgess, G.C., Harms, M.P., Petersen, S.E., Schlaggar, B.L., Corbetta, M., Glasser, M.F., Curtiss, S., Dixit, S., Feldt, C., Nolan, D., Bryant, E., Hartley, T., Footer, O., Bjork, J.M., Poldrack, R., Smith, S., Johansen-Berg, H., Snyder, A.Z., Van Essen, D.C., 2013. WU-Minn HCP Consortium. Function in the human connectome: task-fmri and individual differences in behavior. *Neuroimage* 80, 169–189.
- Bardaweel, S.K., Alzweiri, M., Ishaqat, A.A., 2014. D-Serine in neurobiology: cns neurotransmission and neuromodulation. *Can. J. Neurol. Sci.* 41 (2), 164–176.
- Barlow, H.B., Kohn, H.I., Walsh, E.G., 1947. The effect of dark adaptation and of light upon the electric threshold of the human eye. *Am. J. Physiol.* 148, 376–381.
- Basser, P.J., Pierpaoli, C., 2011. Microstructural and physiological features of tissues elucidated by quantitative-diffusion-tensor MRI. *J. Magn. Reson.* 213, 560–570. (PubMed: 22152371).
- Berry, M.V., Geim, A.K., 1997. Of flying frogs and levitrons. *Eur. J. Phys.* 18, 307–313.
- Bird, M.D., Dixon, I.R., Toth, J., Large, 2015. High-field magnet projects at the NIMFL. *IEEE Trans. Appl. Supercond.* 25 (3), 4300606.
- Bizzi, A., Brooks, R.A., Brunetti, A., Hill, J.M., Alger, J.R., Miletich, R.S., Francavilla, T.L., Di Chiro, G., 1990. Role of iron and ferritin in MR imaging of the brain: a study in primates at different field strengths. *Radiology* 177, 59–65. (PubMed: 2399339).
- Brandt, B.L., Hannahs, S., Schneider-Muntau, H.-J., Boebinger, G., Sullivan, N.S., 2001. The National High Magnetic Field Laboratory. *Physica B* 294–295, 505–511.
- Branzoli, F., Techawiboonwong, A., Kan, H., Webb, A., Ronen, I., 2013. Functional diffusion-weighted magnetic resonance spectroscopy of the human primary visual cortex at 7 T. *Magn. Reson. Med.* 69, 303–309. (PubMed: 23165888).
- Bras, W., Diakun, G.P., Díaz, J.F., Maret, G., Kramer, H., Bordas, J., Medrano, F.J., 1998. The susceptibility of pure tubulin to high magnetic fields: a magnetic birefringence and X-ray fiber diffraction study. *Biophys. J.* 74, 1509–1521. (PubMed: 9512047).
- Breuer, J., 1875. Ueber die Function der Bogengänge des Ohrlabyrinths. *Med. Jahrb.* 4, 72–124.
- Brocklehurst, B., McLauchlan, K.A., 1996. Free radical mechanism for the effects of environmental electromagnetic fields on biological systems. *Int. J. Radiat. Biol.* 69, 3–24. (PubMed: 8601753).
- Budinger, T.F., 1979. Thresholds for physiological effects due to RF and magnetic fields used in NMR imaging. *IEEE Trans. Nucl. Sci.* 26, 2821–2825.
- Budinger, T.F., 2016. The Many Dimensions of Concussion. *The Bridge* 46. National Acad. Sciences, Wash. DC, 3–22.
- Budinger, T.F., Lyman, J.T., Tobias, C.A., 1972. Visual perception of accelerated nitrogen nuclei interacting with the human retina. *Nature* 239, 209–212. (PubMed: 4562730).
- Budinger T.F., Cullander C., Bordow R., 1984. Switched magnetic field thresholds for the induction of magnetophosphenes. In: *Proceedings Annual Meeting Society Mag Res Medicine. Soc Mag Res in Medicine*, New York, vol. 118.
- Budinger, T.F., Fischer, H., Hentschel, D., Reinfelder, H.-E., Schmitt, F., 1991. Physiological effects of fast-oscillating magnetic field gradients. *J. Comput. Assist. Tomogr.* 15, 909–914. (PubMed: 1939767).
- Budinger, T.F., Bird, M.D., Frydman, L., Long, J.R., Mareci, T.H., Rooney, W.D., Rosen, B., Schenck, J.F., Schepkin, V.D., Sherry, A.D., Sodickson, D.K., Springer, C.S., Thulborn, K.R., Uğurbil, K., Wald, L.L., 2016. Toward 20 T magnetic resonance for human brain studies: opportunities for discovery and neuroscience rationale. *Magma* 29, 617–639. (PubMed: 27194154).
- Caeyenberghs, K., Siugzdaite, R., Drijckoning, D., Marinazzo, D., Swinnen, S.P., 2015. Functional connectivity density and balance in young patients with traumatic axonal injury. *Brain Connect* 5 (7), 423–432. <http://dx.doi.org/10.1089/brain.2014.0293>, (Epub2014 Dec 2.[PubMed]: 25327385).
- Cai, R., Yang, H., He, J., Zhu, W., 2009. The effects of magnetic fields on water molecular hydrogen bonds. *J. Mol. Struct.* 938, 15–19.
- Cao, Z., Park, J., Cho, Z.Ä., Collins, C.M., 2015. Numerical evaluation of image homogeneity, signal-to-noise ratio, and specific absorption rate for human brain imaging at 1.5, 3, 7, 10.5, and 14 T in an 8-channel transmit/receive array. *J. Magn. Reson. Imaging* 41 (5), 1432–1439.
- Cason, A.M., Kwon, B.S., Smith, J.C., Houpt, T.A., 2009. Labyrinthectomy abolishes the behavioral and neural response of rats to a high-strength static magnetic field. *Physiol. Behav.* 97, 36–43. (PubMed: 19419674).
- Chakeres, D.W., Kangaru, A., Boudoulas, H., Young, D.C., 2003. Effect of static magnetic field exposure of up to 8 T on sequential human vital sign measurements. *J. Magn. Reson. Imaging* 18, 346–352.
- Chen, J.P., Bai, H., Bird, M.D., Bole, S., Cantrell, K., Toth, J., Zhai, Y., 2010. Cryostat design for the HZB and NIMFL series-connected hybrids. *IEEE Trans. Appl. Supercond.* 20 (3), 688–691.
- Cho, Z.H., Park, S.H., Kim, J.H., Chung, S.C., Chung, S.T., Chung, J.Y., Moon, C.W., Yi, J.H., Sin, C.H., Wong, E.K., 1997. Analysis of acoustic noise in MRI. *Magn. Reson. Imaging* 15 (7), 815–822.
- Choi, C., Dimitrov, I., Douglas, D., Zhao, C., Hawesa, H., Ghose, S., Tamminga, C.A., 2009a. In vivo detection of serine in the human brain by proton magnetic resonance spectroscopy (1H-MRS) at 7 T. *Magn. Reson. Med.* 62 (4), 1042–1046.
- Choi, C., Douglas, D., Hawesa, H., Jindal, A., Storey, C., Dimitrov, I., 2009b. Measurement of glycine in human prefrontal brain by point-resolved spectroscopy at 7.0 T in vivo. *Magn. Reson. Med.* 62, 1305–1310.
- Cocchi, L., Harding, I.H., Lord, A., Pantelis, C., Yucel, M., Zalesky, A., 2014. Disruption of structure-function coupling in the schizophrenia connectome. *Neuroimage Clin.* 4, 779–787. <http://dx.doi.org/10.1016/j.nicl.2014.05.004>. PMID:24936428.
- Colon-Perez, L.M., King, M., Parekh, M., Boutzoukas, A., Carmona, E., Couret, M., Klassen, R., Mareci, T.H., Carney, P.R., 2015. Highfield magnetic resonance imaging of the human temporal lobe. *Neuroimage Clin.* 9, 58–68. (PubMed: 26413472).
- Costagli, M., Symms, M.R., Angeli, L., Kelley, D.A., Biagi, L., Farnetani, A., Rua, C., Donatelli, G., Tiberi, G., Tosetti, M., Cosottini, M., 2016. Assessment of Silent T1-weighted head imaging at 7 T. *Eur. Radiol.* 26, 1879–1888. (PubMed: 26318369).
- d'Arsonval, A., 1896. Dispositifs pour la mesure des courants alternatifs de toutes fréquences. *C. R. Soc. Biol.* 2, 450–451.
- de la Fuente-Sandoval, C., Leon-Ortiz, P., Azcarraga, M., Stephano, S., Favila, R., Diaz-Galvis, L., Alvarado-Alanis, P., Ramirez-Bermudez, J., Graff-Guerrero, A., 2013. Glutamate levels in the associative striatum before and after 4 weeks of antipsychotic treatment in first-episode psychosis: a longitudinal proton magnetic resonance spectroscopy study. *JAMA Psychiatry* 70, 1057–1066. (PubMed: 23966023).
- De Martino, F., Moerel, M., Uğurbil, K., Goebel, R., Yacoub, E., Formisano, E., 2015. Frequency preference and attention effects across cortical depths in the human primary cortex. *Proc. Natl. Acad. Sci. USA* 112, 16036–16041. (PubMed: 26668397).
- den Ouden, A., Wulfer, C.A., Hussey, N.E., Laureijs, G., Wijnen, F.J.P., Wulterkens, G.F.A.J., Bird, M.D., Dixon, I.R., Peerenboom, J.A.A.J., 2016. Progress in the development of the HFML 45 T hybrid magnet. *IEEE Trans. Appl. Supercond.* 26 (4), 4301807. <http://dx.doi.org/10.1109/TASC.2016.2524544>.
- Denegre, J.M., Valles, J.M., Jr, Lin, K., Jordan, W.B., Mowry, K.L., 1998. Cleavage planes in frog eggs are altered by strong magnetic fields. *Proc. Natl. Acad. Sci. USA* 95, 14729–14732. (PubMed: 9843957).
- Dixon, I.R., Adkins, T.A., Bird, M.D., Bole, S.T., Toth, J., Ehmler, H., Heinrich, H.J., Hoffman, M., Kempfer, S., Smeibile, P., 2017. Commissioning of the series-connected hybrid magnet for the Helmholtz Zentrum Berlin Neutron Scattering Center. *IEEE Trans. Appl. Supercond.*, 26, (in press).
- Duyn, J.H., 2012. The future of ultra-high field MRI and fMRI for study of the human brain. *Neuroimage* 62 (2), 1241–1248.
- Duyn, J.H., Schenck, J., 2016. Contributions to magnetic susceptibility of brain tissue. *NMR Biomed.* 2016. <http://dx.doi.org/10.1002/nbm.3546>, (Epub ahead of print).
- Duyn, J.H.I., van Gelderen, P., Li, T.Q., de Zwart, J.A., Koretsky, A.P., Fukunaga, M., 2007. High-field MRI of brain cortical substructure based on signal phase. *Proc. Natl. Acad. Sci. USA* 104 (28), 11796–11801.
- Elabayad, I.A., Kalayciyan, R., Shambhag, N.C., Schad, L.R., 2014. In vivo detection of serine in the human brain by proton magnetic resonance spectroscopy (1H-MRS) at 7 T. *IEEE Trans. Biomed. Eng.* 61 (2), 334–345.
- Errico, F., Napolitano, F., Squillace, M., Vitucci, D., Blasi, G., de Bartolomeis, A., Bertolino, A., D'Aniello, A., Usiello, A., 2013. Decreased levels of D-aspartate and NMDA in the prefrontal cortex and striatum of patients with schizophrenia. *J. Psychiatr. Res.* 47 (10), 1432–1437.
- Fatahi, M., Reddig, A., Vijayalaxmi Friebe, B., Hartig, R., Prihoda, T.J., Ricke, J., Roggenbuck, D., Reinhold, D., Speck, O., 2016. DNA double-strand breaks and micronuclei in human bloodlymphocytes after repeated whole body exposures to 7T Magnetic Resonance Imaging. *Neuroimage*. <http://dx.doi.org/10.1016/j.neuroimage.2016.03.023>.
- Fitzpatrick, R.C., Day, B.L., 2004. Probing the human vestibular system with galvanic stimulation. *J. Appl. Physiol.* 96, 2301–2316. (PubMed: 15133017).
- Fleysher, L., Oesingmann, N., Brown, R., Sodickson, D.K., Wiggins, G.C., Ingles, M.,

2013. Noninvasive quantification of intracellular sodium in human brain using ultrahigh-field MRI. *NMR Biomed.* 26, 9–19. (PubMed: 2714793).
- Ford, A.A., Colon-Perez, L., Triplett, W.T., Gullett, J.M., Mareci, T.H., FitzGerald, D.B., 2013. Imaging white matter in human brainstem. *Front Hum Neurosci.* 7, 400. (PubMed: 23898254).
- Foster, K., Moulder, J., Budinger, T.F., 2017. Will an MRI examination damage your genes? *Radiat. Res. (Comment.)* 187 (1), 1–6. <http://dx.doi.org/10.1667/RR14529.1>.
- Francati, V., Vermetten, E., Bremner, J., 2007. Functional neuroimaging studies in posttraumatic stress disorder: review of current methods and findings. *Depress. Anxiety* 24 (3), 202–218. (1091-4269) [Ser. online].
- Fukunaga, M., Li, T.-Q., van Gelderen, P., de Zwart, J.A., Shmueli, K., Yao, B., Lee, J., Maric, D., Aronova, M.A., Zhang, G., Leapman, R.D., Schenck, J.F., Merkle, H., Duyn, J.H., 2010. Layer-specific variation of iron content in cerebral cortex as a source of MRI contrast. *Proc. Natl. Acad. Sci. USA* 107, 3834–3839. (PubMed: 20133720).
- Gao, F., Edden, R.A., Li, M., Puts, N.A., Wang, G., Liu, C., Zhao, B., Wang, H., Bai, X., Zhao, C., Wang, X., Barker, P.B., 2013. Edited magnetic resonance spectroscopy detects an age-related decline in brain GABA levels. *Neuroimage* 78, 75–82. (PubMed: 23587685).
- Ghodbane, S.I., Lahbib, A., Sakly, M., Abdelmelek, H., 2013. Bioeffects of static magnetic fields: oxidative stress, genotoxic effects, and cancer studies. *Biomed. Res. Int.* 602987. (PubMed: 24027759).
- Giovannelli, L., Pitozzi, V., Moretti, S., Boddi, V., Dolara, P., 2006. Seasonal variations of DNA damage in human lymphocytes: correlation with different environmental variables. *Mutat. Res.* 593 (1–2), 143–152.
- Goa, P.E., Koopmans, P.J., Poser, B.A., Barth, M., Norris, D.G., 2014. BOLD fMRI signal characteristics of S1- and S2-SSFP at 7 T. *Front. Neurosci.* 8, 49. (PubMed: 24659952).
- Godeke, D., Cheng, D., Dietrich, D.R., English, C.D., Felice, H., Hannaford, C.R., Prestemon, S.O., Sabbi, G., Scanlan, R.M., Hikichi, Y., Nishioka, J., Hasegawa, T., 2008. Development of wind-and-react bi-2212 accelerator magnet technology. *IEEE Trans. Appl. Supercond.* 18, 516–519.
- Goff, D.C., Bottiglieri, T., Arning, E., Shih, V., Freudenreich, O., Evins, A.E., Henderson, D.C., Baer, L., Coyle, J., 2004. Folate, homocysteine, and negative symptoms in schizophrenia. *Am. J. Psychiatry* 161 (9), 1705–1708. (PubMed: 15337665).
- Goldman, A., Grossman, W.E., Friedlander, P.C., 1989. Reduction of sound levels with anti-noise in MR imaging. *Radiology* 173, 549–550. (PubMed: 2798889).
- Gordji-Nejad, A., Möllenhoff, K., Oros-Peusquens, A.M., Pillai, D.R., Shah, N.J., 2014. Characterizing cerebral oxygen metabolism employing oxygen-17 MRI/MRS at high fields. *MAGMA* 27, 81–93. (PubMed: 24337392).
- Gorgolewski, K.J., Mendes, N., Wilfing, D., Wladimirov, E., Gauthier, C.J., Bonnen, T., Ruby, F.J., Trampel, R., Bazin, P.L., Cozart, R., Smallwood, J., Margulies, D.S., 2015. A high resolution 7-Tesla resting-state fMRI test-retest dataset with cognitive and physiological measures. *Sci. Data* 2, 140054. (PubMed: 25977805).
- Guivel-Scharen, V., Sinnwell, T., Wolff, S.D., Balaban, R.S., 1998. Detection of proton chemical exchange between metabolites and water in biological tissues. *J. Magn. Reson.* 133, 36–45. (PubMed: 9654466).
- Gukovskaya, A.S., Pulido, H.A., Zinchenko, V.P., Evtodienko, Yu.V., 1989. Inhibitors of arachidonic acid metabolism eliminate the increase in cytosolic free calcium induced by the mitogen concanavalin A in rat thymocytes. *FEBS Lett.* 244, 461–464. (PubMed: 2493398).
- Guo, W.I., Liu, F., Xiao, C., Zhang, Z., Liu, J., Yu, M., Zhang, J., Zhao, J., 2015. Decreased insular connectivity in drug-naïve major depressive disorder at rest. *J. Affect. Disord.* 179, 31–37. <http://dx.doi.org/10.1016/j.jad.2015.03.028>. (Epub2015 Mar 24).
- Haacke, E.M., Mittal, S., Wu, Z., Neelavalli, J., Cheng, Y.C., 2009. Susceptibility-weighted imaging: technical aspects and clinical applications, part 1. *AJNR Am. J. Neuroradiol.* 30 (1), 19–30. <http://dx.doi.org/10.3174/ajnr.A1400>.
- Hattori, Y., Fukatsu, H., Ishigaki, T., 2007. Measurement and evaluation of the acoustic noise of a 3 T MR scanner. *Nagoya J. Med. Sci.* 69, 23–38. (PubMed: 17378177).
- Heidemann, R.M., Anwander, A., Feiweier, T., Knösche, T.R., Turner, R., 2012. k-space and q-space: combining ultra-high spatial and angular resolution in diffusion imaging using ZOOPPA at 7T. *Neuroimage* 60 (2), 967–978. (PubMed: 22245337).
- Hoffmann, S.H., Begovatz, P., Nagel, A.M., Umathum, R., Schommer, K., Bachert, P., Bock, M., 2011. A measurement setup for direct ¹⁷O MRI at 7 T. *Magn. Reson. Med.* 66, 1109–1115. (PubMed: 21394777).
- Hollenberg, P.F., 1992. Mechanisms of cytochrome P450 and peroxidase-catalyzed xenobiotic metabolism. *FASEB J.* 6, 686–694. (PubMed: 1537457).
- Hong, F.T., 1995. Magnetic field effects on biomolecules, cells, and living organisms. *Biosystems.* 36, 187–229. (PubMed: 16106367).
- Hoult, D.I., Richards, R., 1976. The signal-to-noise ratio of the nuclear magnetic resonance experiment. *J. Magn. Reson.* 24, 71–85. (PubMed: 22152352).
- Houpt, T.A., Cassell, J.A., Riccardi, C., DenBleyker, M.D., Hood, A., Smith, J.C., 2007. Rats avoid high magnetic fields: dependence on an intact vestibular system. *Physiol. Behav.* 92, 741–747. (PubMed: 17585969).
- Houpt, T.A., Carella, L., Gonzalez, D., Janowitz, I., Mueller, A., Mueller, K., Neth, B., Smith, J.C., 2011. Behavioral effects on rats of motion within a high static magnetic field. *Physiol. Behav.* 102, 338–346. (PubMed: 21118699).
- Iima, M., Le Bihan, D. Diffusion magnetic resonance imaging: what water tells us about biological tissues. *PLoS Biol.* 13(7) e1002203. doi: <http://dx.doi.org/10.1371/journal.pbio.1002202>.
- Imagawa, S., Chikaraishi, H., Obana, T., Takada, S., Yanagi, N., 2017. Quench protection system for a 13 T magnet with a 700 mm bore. *IEEE Trans. Appl. Supercond.* 26, (in press).
- International Technological Commission, 2015. IEC 60601-2-33:2010+AMD1:2013+AMD2:2015 CSV. Medical electrical equipment - Part 2-33: particular requirements for the basic safety and essential performance of magnetic resonance equipment for medical diagnosis, 540 pp.
- Irnich, W., Schmitt, F., 1995. Magnetostimulation in MRI. *Magn. Reson. Med.* 33, 619–623. (PubMed: 7596265).
- Jones, C.K., Polders, D., Hua, J., Hoogduin, H.J., Zhou, J., van Zijl, P.C.M., 2012. In Vivo 3D whole-brain pulsed steady state chemical exchange saturation transfer at 7T. *Magn. Reson. Med.* 67, 1579–1589. (PubMed: 22083645).
- Jones, C.K., Huang, A., Xu, J., Edden, R.A., Schär, M., Hua, J., Oskolkov, N., Zacà, D., Zhou, J., McMahon, M.T., Pillai, J.J., van Zijl, P.C., 2013. Nuclear overhauser enhancement (NOE) imaging in the human brain at 7T. *Neuroimage* 77, 114–124. (PubMed: 23567889).
- Jones, D.K., Knösche, T.R., Turner, R., 2013. White matter integrity, fiber count, and other fallacies: the do's and don'ts of diffusion MRI. *Neuroimage* 73, 239–254. (PubMed: 22846632).
- Kangarlou, A., Burgess, R.E., Zhu, H., Nakayama, T., Hamlin, R.L., Abduljalil, A.M., Robitaille, P.M.L., 1999. Cognitive, cardiac, and physiological safety studies in ultra high field magnetic resonance imaging. *Magn. Reson. Imaging* 17, 1407–1416. (PubMed: 10609989).
- Keltner, J.R., Roos, M.S., Brakeman, P.R., Budinger, T.F., 1990. Magneto-hydrodynamics of blood flow. *Magn. Reson. Med.* 16, 139–149. (PubMed: 2255234).
- Keltner, J.R., Carlson, J.W., Roos, M.S., Wong, S.T., Wong, T.L., Budinger, T.F., 1991. Electromagnetic fields of surface coil in vivo NMR at high frequencies. *Magn. Reson. Med.* 22, 467–480. (PubMed: 1812380).
- Kiehl, K.A., Smith, A.M., Hare, R.D., Mendrek, A., Forster, B.B., Brink, J., Liddle, P.F., 2001. Limbic abnormalities in affective processing by criminal psychopaths as revealed by functional magnetic resonance imaging. *Biol. Psychiatry* 50 (9), 677–684.
- Kirov, I.I., Hardy, C.J., Matsuda, K., Messinger, J., Cankurtaran, C.Z., Warren, M., Wiggins, G.C., Perry, N.N., Babb, J.S., Goetz, R.R., George, A., Malaspina, D., Gonen, O., 2013. In vivo 7 T imaging of the dentate granule cell layer in schizophrenia. *Schizophr. Res.* 147 (2–3), 362–367. <http://dx.doi.org/10.1016/j.schres.2013.04.020>.
- Kirsch, S., Augath, M., Seiffge, D., Schilling, L., Schad, L.R., 2010. In vivo chlorine-35, sodium-23 and proton magnetic resonance imaging of the rat brain. *NMR Biomed.* 23 (6), 592–600.
- Kirschvink, J.L., Kobayashi-Kirschvink, A., Woodford, B.J., 1992. Magnetite biomineralization in the human brain. *Proc. Natl. Acad. Sci. USA* 89, 7683–7687.
- Kiyatkin, E.A., Lenoir, M., 2012. Rapid fluctuations in extracellular brain glucose levels induced by natural arousing stimuli and intravenous cocaine: fueling the brain during neural activation. *J. Neurophysiol.* 108, 1669–1684. (PubMed: 22723672).
- Larbalestier, D.C., Jiang, J., Trociewicz, U.P., Kametani, F., Scheuerlein, C., Dalban-Canassy, M., Matras, M., Chen, P., Craig, N.C., Lee, P.J., Hellstrom, E.E., 2014. Isotropic round-wire multifilament cuprate superconductor for generation of magnetic fields above 30 T. *Nat. Mater.* 13, 375–381. (PubMed: 24608141).
- Lattanzi, R., Sodickson, D.K., Grant, A.K., Zhu, Y., 2009. Electrodynamics constraints on homogeneity and radiofrequency power deposition in multiple coil excitations. *Magn. Reson. Med.* 61, 315–334. (PubMed: 19165885).
- Lattanzi, R., Wiggins, G.C., Zhang, B., Duan, Q., Brown, R., Sodickson, D.K., 2017. Approaching ultimate intrinsic signal-to-noise ratio with loop and dipole antennas. *Magn. Reson. Med.*, in press.
- Le Bihan, D., Johansen-Berg, H., 2012. Diffusion MRI at 25: exploring brain tissue structure and function. *Neuroimage* 61, 324–341. (PubMed: 22120012).
- Le Bihan, D., Breton, E., Lallemand, D., Grenier, P., Cabanis, E., Laval Jeantet, M., 1986. MR imaging of intravoxel incoherent motions: application to diffusion and perfusion in neurologic disorders. *Radiology* 161, 401–407. (PubMed: 3763909).
- Leuze, C.W., Anwander, A., Bazin, P.L., Dhital, B., Stüber, C., Reimann, K., Geyer, S., Turner, R., 2014. Layer-specific intracortical connectivity revealed with diffusion MRI. *Cereb. Cortex* 24, 328–339. (PubMed: 23099298).
- Li, M., Schiano, J.L., Samra, J.E., Shetty, K.K., Brey, W.W., 2011. Reduction of magnetic field fluctuations in powered magnets for NMR using inductive measurements and sampled-data feedback control. *J. Magn. Reson.* 212 (2), 254–264.
- Lövsund, P., Öberg, P.A., Nilsson, S.E.G., 1980. Magnetophosphores: a quantitative analysis of thresholds. *Med. Biol. Eng. Comput.* 18, 326–334. (PubMed: 6968384).
- Lu, A., Atkinson, I.C., Zhou, X.J., Thulborn, K.R., 2013. PCr/ATP ratio mapping of the human head by simultaneously imaging of multiple spectral peaks with interleaved excitations and flexible twisted projection imaging readout trajectories at 9.4 T. *Magn. Reson. Med.* 69, 538–544. (PubMed: 22529019).
- Lu, M., Zhang, Y., Uğurbil, K., Chen, W., Zhu, X.H., 2010. In vitro and in vivo studies of 17O NMR sensitivity at 9.4 and 16.4 T. *Magn. Reson. Med.* 69 (6). <http://dx.doi.org/10.1002/mrm.24386>.
- Lvovsky, Y., Stautner, E.W., Zhang, Z., 2013. Novel technologies and configuration of superconducting magnets for MRI. *Supercond. Sci. Technol.* 26, 93001–93071.
- Maclaren, J.I., Armstrong, B.S., Barrows, R.T., Danishad, K.A., Ernst, T., Foster, C.L., Gumus, K., Herbst, M., Kadashevich, I.Y., Kusik, T.P., Li, Q., Lovell-Smith, C., Prieto, T., Schulze, P., Speck, O., Stucht, D., Zaitsev, M., 2012. Measurement and correction of microscopic head motion during magnetic resonance imaging of the brain. *PLoS One* 7 (11), e48088. <http://dx.doi.org/10.1371/journal.pone.0048088>.
- Macovski, A., 1996. Noise in MRI. *Magn. Reson. Med.* 36, 494–497. (PubMed: 8875425).
- Majkic, G., Galstyan, E., Selvamannickam, V., 2010. High performance 2G-HTS wire using a novel MOCVD system. *Appl. Supercond. IEEE Trans. Supercond.* 25, 1–4.
- Mansfield, P., Harvey, P.R., 1993. Limits to neural stimulation in echo-planar imaging. *Magn. Reson. Med.* 29, 746–758.
- Mansfield, P., Chapman, B.L., Bowtell, R., Glover, P., Coxon, R., Harvey, P.R., 1995. Active acoustic screening reduction of noise in gradient coils by Lorentz force balancing. *Magn. Reson. Med.* 33, 271–281. (PubMed: 7707921).

- Marg, E., 1991. Magnetostimulation of Vision: direct noninvasive stimulation of the retina and the visual brain. *Optom. Vision Sci.* 68, 427–440. (PubMed: 1891194).
- Markiewicz, W.D., Dixon, I.R., Swenson, C.A., Marshall, W.S., Painter, T.A., Bole, S.T., Cosmus, T., Parizh, M., King, M., Ciancetta, G., 2000. 900 MHz wide bore NMR spectrometer magnet at NHMFL. *IEEE Trans. Appl. Supercond.* 10, 728–731.
- Martovetsky, N., Michael, P., Minervini, J., Radovinsky, A., Takayasu, M., Thome, R., Ando, T., Isono, T., Kato, T., Nakajima, N., Nishijima, G., Nunoya, Y., Sugimoto, M., Takahashi, Y., Tsuji, H., Bessette, D., Okuno, K., Ricci, M., 2001. ITER CS model coil and CS insert test results. *IEEE Trans. Appl. Supercond.* 11, 2030–2033.
- Martovetsky, N., 2015. Personal communication to Mark Bird.
- McIntyre, C.C., Grill, W.M., 2002. Extracellular stimulation of central neurons: influence of stimulus waveform and frequency on neuronal output. *J. Neurophysiol.* 88 (4), 1592–1604.
- McNab, J.A., Edlow, B.L., Witzel, T., Huang, S.Y., Bhat, H., Heberlein, K., Feiweier, T., Liu, K., Keil, B., Cohen-Adad, J., Tisdall, M.D., Folkerth, R.D., Kinney, H.C., Wald, L.L., 2013. The Human Connectome Project and beyond: initial applications of 3.0 mT/m gradients. *Neuroimage* 80, 234–245. (PubMed: 23711537).
- Mian, O.S., Li, Y., Antunes, A., Glover, P.M., Day, B.L., 2016. Effect of head pitch and roll orientations on magnetically induced vertigo. *J. Physiol.* 594 (4), 1051–1067.
- Miller, J.R., Bird, M.D., Bonito-Oliva, A., Eyssa, Y., Kenney, W.J., Painter, T., Schneider-Muntau, H.-J., Summers, L.T., Van Sciver, S.W., Welton, S., Wood, R.J., Williams, J.E.C., Bobrov, E., Iwasa, Y., Leupold, M., Stejskal, V., Weggel, R., 1994. An overview of the 45 T hybrid magnet system for the New National High Magnetic Field Laboratory. *IEEE Trans. Magn.* 30, 1563–1571.
- Moelker, A., Wielopolski, P.A., Pattynama, P.M.T., 2003. Relationship between magnetic field strength and magnetic-resonance-related acoustic noise levels. *Magn. Reson. Mater. Phys. Biol. Med.* 16 (1), 52–55.
- Muckli, L., De Martino, F., Vizoli, L., Petro, L.S., Smith, F.W., Uğurbil, K., Goebel, R., Yacoub, E., 2015. Contextual feedback to superficial layers of V1. *Curr. Biol.* 25, 2690–2695. (PubMed: 26441356).
- Nagel, A.M., Lehmann-Horn, F., Weber, M.A., Jurkat-Rott, K., Wolf, M.B., Radbruch, A., Umathum, R., Semmler, W., 2014. In vivo ³⁵Cl MR imaging in humans: a feasibility study. *Radiology* 271, 585–595. (PubMed: 24495267).
- Nagel, A.M., Umathum, R., Rösler, M.B., Ladd, M.E., Litvak, I., Gor'kov, P.L., Brey, W.W., Schepkin, V.D., 2016. (39) K and (23) Na relaxation times and MRI of rat head at 21.1 T. *NMR Biomed.* 29, 759–766. (PubMed: 27061712).
- Nakashima, T., Yamazaki, K., Kobayashi, S., Kagiya, T., Kikuchi, M., Takeda, S., Osabe, G., Fujikami, J., Osamura, J., 2015. Drastic improvement in mechanical properties of DI-BSCCO wire with novel lamination material. *IEEE Trans. Appl. Supercond.* 25, 1–5.
- Nasr, S., Polimeni, J.R., Tootell, R.B., 2016. Interdigitated color and disparity-selective columns within human visual cortical areas V2 and V3. *J. Neurosci.* 36, 1841–1857. (PubMed: 26865609).
- National Research Council, 2013. High Magnetic Field Science and Its Application in the United States: Current Status and Future Directions, Wash. D.C. 2000.
- New, P.F., Rosen, B.R., Brady, T.J., Buonanno, F.S., Kistler, J.P., Burt, C.T., Hinshaw, W.S., Newhouse, J.H., Pohost, G.M., Taveras, J.M., 1983. Potential hazards and artifacts of ferromagnetic and nonferromagnetic surgical and dental materials and devices in nuclear magnetic resonance imaging. *Radiology* 147 (1), 139–148.
- Nishiyama, Y., Pandey, M., Florian, P., Fyon, F., Hashi, K., Ohki, S., Nishijima, G., Matsumoto, S., Noguchi, T., Deguchi, T., Gotom, A., Shimizu, T., Maeda, H., Takahashi, M., Yanagisawa, Y., Tanaka, R., Nemoto, T., Miyamoto, T., Suematsu, H., Saito, K., Miki, T., 2015. 1020 MHz LTS/HTS NMR: II. Application to solid-state NMR. Presented at Proceedings of the 56th Experimental Nuclear Magnetic Resonance Conference (ENC), Asilomar, CA, April 19–24.
- Nitsche, M.A., Cohen, L.G., Wassermann, E.M., Priori, A., Lang, N., Antal, A., Paulus, W., Hummel, F., Boggio, P.S., Fregni, F., Pascual-Leone, A., 2008. Transcranial direct current stimulation: state of the art 2008. *Brain Stimul.* 1 (3), 206–223. (Review.PMID:20633386).
- Nyenhuis, J.A., Bourland, J.D., Schaefer, D.J., 1997. Analysis from a stimulation perspective of the field patterns of magnetic resonance imaging gradient coils. *J. Appl. Phys.* 81, 4314–4316.
- Nyenhuis, J.A., Park, S.-M., Kamondetdacha, R., Amjad, A., Shellock, F.G., Rezaei, A.R., 2005. MRI and implanted medical devices: basic interactions with an emphasis on heating. *IEEE Trans. Devices Mater. Reliab.* 5, 467–480.
- Ogawa, S., Tank, D.W., Menon, R., Ellermann, J.M., Kim, S.G., Merkle, H., Uğurbil, K., 1992. Intrinsic signal changes accompanying sensory stimulation: functional brain mapping with magnetic resonance imaging. *Proc. Natl. Acad. Sci. USA* 89 (13), 5951–5955.
- Okano, H., 2008. Effects of static magnetic fields in biology: role of free radicals. *Front. Biosci.* 13, 6106–6125. (PubMed: 18508647).
- Olman, C.A., Harel, N., Feinberg, D.A., He, S., Zang, P., Uğurbil, K., Yacoub, E., 2012. Layer-specific fMRI reflects different neuronal computations at different depths in human V1. *PLoS One* 7, e332536. (PubMed: 22448223).
- Oman, C.M., Young, I.R., 1972. The physiological range of pressure difference and cupula deflections in the human semicircular canal. Theoretical considerations. *Acta Otolaryngol.* 74, 324–331. (PubMed: 4639724).
- Patel, M., Williamsom, R.A., Dorevitch, S., Buchanan, S., 2008. Pilot study investigating the effect of the static magnetic field from a 9.4-T MRI on the vestibular system. *J. Occup. Environ. Med.* 50, 576–583. (PubMed: 18469627).
- Pohmann, R., Speck, O., Scheffler, K., 2016. Signal-to-noise ratio and MR tissue parameters in human brain imaging at 3, 7, and 9.4 T using current receive coil arrays. *Magn. Reson. Med.* 75 (2), 801–809.
- Polenova T. and Budinger T., 2016. Ultrahigh field NMR and MRI: science at a crossroads. Report on a jointly-funded NSF, NIH and DOE workshop, held on November 12-13, 2015 in Bethesda, Maryland, USA. *J. Magn. Reson.* 266, 81-6. <http://dx.doi.org/10.1016/j.jmr.2016.01.008>. Epub 2016 Jan 22.
- Qiao, H., Zhang, X., Zhu, X.H., Du, F., Chen, W., 2006. In vivo 31P MRS of human brain at high/ultrahigh fields: a quantitative comparison of NMR detection sensitivity and spectral resolution between 4 T and 7 T. *Magn. Reson. Imaging* 24 (10), 1281–1286.
- Rausch, M., Gebhardt, M., Kaltenbacher, M., Landes, H., 2005. Computer-aided design of clinical magnetic resonance imaging scanners by coupled magnetomechanical-acoustic modeling. *IEEE Trans. Magn.* 41 (1), 72–81.
- Reilly, J.P., 1998. Maximum pulsed electromagnetic field limits based on peripheral nerve stimulation: application to IEEE/ANSI C95.1 electromagnetic field standards. *IEEE Trans. Biomed. Eng.* 45, 137–141. (PubMed: 9444851).
- Roberts, D.C., Marcelli, V., Gillen, J.S., Carey, J.P., Della Santina, C.C., Zee, D.S., 2011. MRI magnetic field stimulates rotational sensors of the brain. *Curr. Biol.* 21 (19), 1635–1640.
- Roland, L.M., Bustillo, J.R., Mullins, P.G., Jung, R.E., Lenroot, R., Landgraf, E., Barrow, R., Yeo, R., Lauriello, J., Brooks, W.M., 2005. Effects of ketamine on anterior cingulate glutamate metabolism in healthy humans: a 4-T proton MRS study. *Am. J. Psychiatry.* 162, 394–396. (PubMed: 15677610).
- Rooney, W., Sammi, M., Grinstead, J., Pollaro, J., Selzer, A., Li, X., Springer, C., 2013. Contrast reagent detection sensitivity increases with B₀: 3 T and 7 T comparison of the human head. In: Proceedings of the International Society for Magnetic Resonance in Medicine, 21, 1224.
- Rooney, W.D., Johnson, G., Li, X., Cohen, E.R., Kim, S.-G., Uğurbil, K., Springer, C.S., 2007. Magnetic field and tissue dependences of human brain longitudinal ¹H₂O relaxation in vivo. *Magn. Reson. Med.* 57, 308–318. (PubMed: 17260370).
- Rooney, W.D., Li, X., Sammi, M.K., Bourdette, D.N., Neuwelt, E.A., Springer, C.S., 2015. Mapping human brain capillary water lifetime: high-resolution metabolic neuroimaging. *NMR Biomed.* 28, 607–623. (PubMed: 25914365).
- Röschmann, P., 1987. Radiofrequency penetration and absorption in the human body: limitations to high-field whole-body nuclear magnetic resonance imaging. *Med Phys.* 14 (6), 922–931.
- Röschmann, P., 1991. Human auditory system response to pulsed radio frequency energy in RF coils for magnetic resonance at 2.4 to 170 MHz. *Magn. Res. Med.* 21, 197–215. (PubMed: 1745119).
- Rossi, S., Hallett, M., Rossini, P.M., Pascual-Leone, A., Safety of TMS Consensus Group, 2009. Safety, ethical considerations, and application guidelines for the use of transcranial magnetic stimulation in clinical practice and research. *Clin. Neurophysiol.* 120 (12), 2008–2039. <http://dx.doi.org/10.1016/j.clinph.2009.08.016>. (Epub 2009 Oct 14).
- Roth, B.J., Basser, P.J., 2009. Mechanical model of neural tissue displacement during Lorentz effect imaging. *Magn. Reson. Med.* 61, 59–64.
- Roth, Y., Amir, A., Levkovitz, Y., Zangen, A., 2007. Three-dimensional distribution of the electric field induced in the brain by transcranial magnetic stimulation using figure 8 and deep h-coils. *J. Clin. Neurophysiol.* 24, 31–38.
- Saedisoemla, A., Djalali, M., Moghadam, A.M., Ramezankhani, O., 2011. Najmi L.2011. Folate and vitamin B12 status in schizophrenic patients. *J. Res. Med. Sci. (Suppl. 1)*, (S437-41).
- Sargent, T., III, Kusubov, N., Taylor, S.E., Budinger, T.F., 1992. Tracer kinetic evidence for abnormal methyl metabolism in schizophrenia. *Biol. Psychiatry* 32, 1078–1090. (PubMed: 1477188).
- Scaiano, J.C., 1995. Exploratory laser flash photolysis study of free radical reactions and magnetic field effects in Melatonin chemistry. *J. Pineal Res.* 19, 189–195. (PubMed: 8789250).
- Schenck, J.F., 1996. The role of magnetic susceptibility in magnetic resonance imaging: mri magnetic compatibility of the first and second kinds. *Med. Phys.* 23, 815–850. (PubMed: 8798169).
- Schenck, J.F., 2005. Physical interactions of static magnetic fields with living tissues. *Prog. Biophys. Mol. Biol.* 87, 185–204. (PubMed: 15556658).
- Schenck, J.F., Dumoulin, C.L., Redington, R.W., Kressel, H.Y., Elliott, R.T., McDougall, L.L., 1992. Human exposure to 4.0-Tesla magnetic fields in a whole-body scanner. *Med. Phys.* 19, 1089–1098. (PubMed: 1518472).
- Schepkin, V.A., Odintsov, B.M., Litvak, I., Gor'kov, P.L., Brey, W.W., Neubauer, A., Budinger, T.F., 2015. Efficient detection of bound potassium and sodium using TQTPPI pulse sequence. *Proc. Int. Soc. Magn. Reson. Med.* 23, 2375.
- Schepkin, V.D., 2016. Sodium MRI of glioma in animal models at ultrahigh magnetic fields. *NMR Biomed.* 29, 175–186. (PubMed: 26174529).
- Schepkin, V.D., Choy, I.O., Budinger, T.F., Obayashi, D.Y., Taylor, S.E., DeCampi, W.M., Amartur, S.C., Young, J.N., 1998. Sodium TQF NMR and intracellular sodium in isolated crystalloid perfused rat heart. *Magn. Reson. Med.* 39 (4), 557–563.
- Schmitt, F., 2014. (Germany) personal communication to T.F. Budinger.
- Setsompop, K., Alagappan, V., Gagoski, B.A., Potthast, A., Hebrank, F., Fontius, U., Franz Schmitt, F., Wald, L.L., Adalsteinsson, E., 2009. Broadband slab selection with B1+ mitigation at 7 T via parallel spectral-spatial excitation. *Magn. Reson. Med.* 61, 493–500. (PubMed: 19161170).
- Setsompop, K., Kimmlingen, R., Eberlein, E., Witzel, T., Cohen-Adad, J., McNab, J.A., Keil, B., Tisdall, M.D., Hoecht, P., Dietz, P., Cauley, S.F., Tountcheva, V., Mantsch, V., Lenz, V.H., Heberlein, K., Potthast, A., Thein, H., Van Horn, J., Toga, A., Schmitt, F., Lehne, D., Rosen, B.R., Wedeen, V., Wald, L.L., 2013. Pushing the limits of in vivo diffusion MRI for the Human Connectome Project. *Neuroimage* 80, 220–233. (PMCID: PMC3725309).
- Setsompop, K., Feinberg, D.A., Polimeni, J.R., 2016. Rapid brain MRI acquisition techniques at ultra-high fields. (Published online 2 February) *NMR Biomed.*, (Published online 2 February).
- Shellock, F.G., 2016. Reference Manual for Magnetic Resonance Safety, Implants and Devices. Biomedical Research Publishing Group, Los Angeles, 712.
- Shemesh, N., Dumez, J.Á., Frydman, L., 2013. Longitudinal relaxation enhancement in 1H NMR spectroscopy of tissue metabolites via spectrally selective excitation. *Chem.*

- Eur. J. 19, 13002–13008, (PubMed: 24038462).
- Shemesh, N., Rosenberg, J.T., Dumez, J.N., Muniz, J.A., Grant, S.C., Frydman, L., 2014. Metabolic properties in stroked rats revealed by relaxation-enhanced magnetic resonance spectroscopy at ultrahigh fields. *Nat. Commun.* 5, 4958, (PubMed: 25229942).
- Sherry, D., 2017. Personal communication to Thomas F. Budinger.
- Sinnecker, T., Kuchling, J., Dusek, P., Dörr, J., Niendorf, T., Paul, F., Wuerfel, J., 2015. Ultrahigh field MRI in clinical neuroimmunology: a potential contribution to improved diagnostics and personalised disease management. *EPMA J.* 6 (1), 16. <http://dx.doi.org/10.1186/s13167-015-0038-y>, (eCollection 2015).
- Smeibidl, P., Bird, M.D., Ehmler, H., Dixon, I.R., Heinrich, J., Hoffmann, M., Kempfer, S., Bole, S., Toth, J., Prokhnenko, O., Lake, B., 2016. First hybrid magnet for neutron-scattering at Helmholtz Zentrum Berlin. *IEEE Trans. Appl. Supercond.* 25, 1–6.
- Springer, C.S., Li, X., Tudorica, L.A., Oh, N., Roy, S.Y.-C., Chui, A.M., Naik, M.L., Holtorf, M.L., Afzala, A., Rooney, W.D., Huang, W., 2014. Intratumor mapping of intracellular water lifetime: metabolic images of breast cancer? *NMR Biomed.* 27, 760–773, (PubMed: 24798066).
- Steiner, U.E., Ulrich, T., 1989. Magnetic field effects in chemical kinetics and related phenomena. *Chem. Rev.* 89, 51–147.
- Stockmann, J., Wald L., 2017. In vivo B_0 field shimming methods for MRI at 7 T. *Neuroimage* (in this issue).
- Stucht, D., Danishad, K.A., Schulze, P., Godenschweiger, F., Zaitsev, M., Speck, O., 2015. Highest resolution in vivo human brain MRI using prospective motion correction. *PLoS One* 10, e0133921, (PubMed: 26226146).
- Takayasu, M., Chiesa, L., Allen, N.C., Minervini, J.V., 2016. Present status and recent development of the twisted stacked-tape cable (TSTC) conductor. *IEEE Trans. Appl. Supercond.* 26, 6400210.
- Tao, H., Guo, S., Ge, T., Kendrick, K.M., Xue, Z., Liu, Z., Feng, J., 2013. Depression uncouples brain hate circuit. *Mol. Psychiatry* 18 (1), 101–111.
- Tenforde, T.S., 2005. Magnetically induced electric fields and currents in the circulatory system. *Prog. Biophys. Mol. Biol.* 87 (2), 279–288.
- Thelwall, P.E., 2007. Detection of ^{17}O -tagged phosphate by ^{31}P MRS: a method with potential for in vivo studies of phosphorus metabolism. *Magn. Reson. Med.* 57 (6), 1168–1172.
- Thelwall, P.E., Blackband, S.J., Chen, W., 2017. Field dependence of 170 T1, T2 and SNR—in vitro and in vivo studies at 4.7, 11 and 17.6 Tesla. In: *Proc Intl Soc Mag Reson Med (ISMRM)*. Toronto.
- Thielscher, A., Kammer, T., 2004. Electric field properties of two commercial figure-8 coils in TMS: calculation of focality and efficiency. *Clin. Neurophysiol.* 115 (7), 1697–1708.
- Thulborn, K.R., Lui, E., Guntin, J., Jamil, S., Sun, Z., Claiborne, T., Atkinson, I.C., 2017. Quantitative sodium MRI imaging of the human brain at 9.4 T provides assessment of tissue sodium concentration and cell volume fraction during normal ageing. *NMR Biomed.* 29, 137–143, (PubMed: 26058461), this issue.
- Tobias, C.A., Budinger, T.F., Lyman, J.T., 1971. Radiation-induced light flashes observed by human subjects in fast neutron, X-ray and positive pion beams. *Nature* 230, 596–598, (PubMed: 4928670).
- Tomasi, D.G., Wang, R., 2007. Induced magnetic field gradients and forces in the human head in MRI. *J. Magn. Reson. Imaging* 26, 1340–1345, (PubMed: 17969175).
- Trattning, S., Bogner, W., Gruber, S., Szomolanyi, P., Juras, V., Robinson, S., Zbyň, Š., Haneder, S., 2015. Clinical applications at ultrahigh field (7 T). Where does it make the difference? *NMR Biomed.* <http://dx.doi.org/10.1002/nbm.3272>, (Publ. online 12 March 2015).
- Tuch, D.S., Reese, T.G., Wiegell, M.R., Makris, N., Belliveau, J.W., Wedeen, V.J., 2002. High angular resolution diffusion imaging reveals intravoxel white matter fiber heterogeneity. *Magn. Reson. Med.* 48, 577–582, (PubMed: 26226146).
- Turner, R., 2002. How much cortex can a vein drain? Downstream dilution of activation-related cerebral blood oxygenation changes. *Neuroimage* 16 (4), 1062–1067.
- Ueno, S., Okano, H., 2012. Static, low-frequency, and pulsed magnetic fields in biological systems. In: *Electromagnetic Fields in Biological Systems*. Taylor & Francis Group, LLC, 3, pp. 115–196.
- Uğurbil, K., Hu, X., Chen, W., Zhu, X.H., Kim, S.G., Georgopoulos, A., 1999. Functional mapping in the human brain using high magnetic fields. *Philos. Trans. R. Soc. Lond. B Biol. Sci.* 354, 1195–1213, (PubMed: 10466146), this issue.
- Uludag, K., Müller-Bierl, B., Uğurbil, K., 2009. An integrative model for neuronal activity-induced signal changes for gradient and spin echo functional imaging. *NeuroImage* 48, 150–165, (PubMed: 19481163).
- Umatham, R., Rösler, M.B., Nagel, A.M., 2013. In vivo ^{39}K MR imaging of human muscle and brain. *Radiology* 269, 569–576, (PubMed: 23878285).
- Valiron, O., Peris, L., Rikken, G., Schweitzer, A., Saoudi, Y., Remy, C., Job, D., 2005. Cellular disorders induced by high magnetic fields. *J. Magn. Reson. Imaging* 22, 334–340, (PubMed: 16106367).
- Valvassori, S.S., Calixto, K.V., Budni, J., Resende, W.R., Varela, R.B., de Freitas, K.V., Gonçalves, C.L., Streck, E.L., Quevedo, J., 2013. Sodium butyrate reverses the inhibition of Krebs cycle enzymes induced by amphetamine in the rat brain. *J. Neural Transm.* 120, 1737–1742, (PubMed: 23851624).
- van der Laan, D.C., Goodrich, L.F., Noyes, P., Trociewitz, U.P., Godeke, A., Abrahimov, D., Francis, A., Larbaestier, D.C., 2015. Engineering current density in excess of 100 A/mm² at 20 T in CORC magnet cables containing RE-Ba₂Cu₃O₇-8 tapes with 38 μm thick substrates. *Supercond. Sci. Technol.* 28, 124001–124008.
- van Zijl, P.C., Yadav, N., 2011. Chemical exchange saturation transfer (CEST): what is in a name and what isn't? *Magn. Reson. Med.* 65 (4), 927–948.
- van Zijl, P.C., Jones, C.K., Ren, J., Malloy, C.R., Sherry, A.D., 2007. MRI detection of glycogen in vivo by using chemical exchange saturation transfer imaging (glycoCEST). *Proc. Natl. Acad. Sci. USA* 104, 4359–4364, (PubMed: 17360529), this issue.
- Vaughan, T., Delabarre, L., Snyder, C., Tian, J., Akgun, C., Shrivastava, D., Liu, W., Olson, C., Adriany, G., Strupp, J., Andersen, P., Gopinath, A., van de Moortele, P.F., Garwood, M., Uğurbil, K., 2006. 9.4 T human MRI: preliminary results. *Magn. Reson. Med.* 56 (6), 1274–1282.
- Vedrine, P., Aubert, G., Beaudet, F., Belorgey, J., Berriaud, C., Bredy, P., Donati, A., Dubois, O., Gilgrass, G., Juster, F.P., Meuris, C., Molinie, F., Nunio, F., Payn, A., Schild, T., Scola, L., Sinanna, A., 2010. Iseult/INUMAC whole body 11.7 T MRI magnet status. *IEEE Trans. Appl. Supercond.* 20, 696–701.
- Versluis, M.J., Teeuwisse, W.M., Kan, H.E., van Buchem, M.A., Webb, A.G., van Osch, M.J., 2013. Subject tolerance of 7 T MRI examinations. *J. Magn. Reson. Imaging* 38, 722–725, (PubMed: 23150466).
- Vijayalaxmi, F.M., Speck, O., 2015. Magnetic resonance imaging (MRI): a review of genetic damage investigations. *Mutat. Res.* 764, 51–63, (PubMed: 26041266).
- Vilenchik, M.M., Knudson, A.G., 2003. Endogenous DNA doublestrand breaks: production, fidelity or repair, and induction of cancer. *Proc. Natl. Acad. Sci.* 100 (22), 12871–12876.
- Vu, A., Auerbach, E., Lenglet, C., Moeller, S., Sotiropoulos, S.N., Jbabdi, S., Andersson, J., Yacoub, E., Uğurbil, K., 2015. High resolution whole brain diffusion imaging at 7T for the human connectome project. *Neuroimage* 122, 318–331, (PubMed: 26260428).
- Wald, L., Polimeni, J., 2016. Impacting the effect of fMRI noise through hardware and acquisition choices - implications for controlling false positive rates. *Neuroimage*. <http://dx.doi.org/10.1016/j.neuroimage.2016.12.057>, pii: S1053-8119(16)30785-6, [Epub ahead of print].
- Wallacek, J., Budinger, T.F., 1992. Pulsed magnetic field effects on calcium signaling in lymphocytes: dependence on cell status and field intensity. *FEBS Lett.* 314, 351–355.
- Wang, R., Wang, G.J., Goldstein, R.Z., Caparelli, E.C., Volkow, N.D., Fowler, J.S., Tomasi, D., 2010. Induced magnetic force in human heads exposed to 4T MRI. *J. Magn. Reson. Imaging* 31, 815–820, (PubMed: 20373424).
- Watson, A.B., Wright, J.S., Loughman, J., 1973. Electrical thresholds for ventricular fibrillation in man. *Med. J. Aust.* 1 (24), 1179–1182.
- Weijers, H.W., Markiewicz, W.D., Voran, A.J., Gundlach, S.R., Sheppard, W.R., Jarvis, B., Johnson, Z.L., Noyes, P.D., Lu, J., Kandel, H., Ba, H., Gavrilin, A.V., Viouchkov, Y.L., Larbaestier, D.C., Abrahimov, D.V., 2014. Progress in the development of a superconducting 32 T magnet with REBCO high field coils. *Appl. Supercond. IEEE Trans. Supercond.* 24, 1–5.
- Wijenburg, S.A., Yang, S., Fischer, B.A., Rowland, L.M., 2015. In vivo assessment of neurotransmitters and modulators with magnetic resonance spectroscopy: application to schizophrenia. *Neurosci. Biobehav. Rev.* 51, 276–295.
- Wikswio, J.P., Barach, J.P., 1980. An estimate of the steady magnetic field strength required to influence nerve conduction. *IEEE Trans. Biomed. Eng.* 27 (12), 722–723.
- Wilson, M.N., 1983. *Superconducting Magnets*. Oxford Univ. Press, Oxford, 46.
- Winkler, S.A., Wade, T.P., Alejski, A., McKenzie, C., Rutt, B.K., 2015. Lorentz damping and the field dependence of gradient coil vibroacoustics. In: *Proceed. Soc. Magn. Reson. Medicine*. Toronto, 23, 1020, this issue.
- Winter, L., Niendorf, T., 2016. Electrodynamics and radiofrequency antenna concepts for human magnetic resonance at 23.5 T (1 GHz) and beyond. *Magn. Reson. Mater. Phys.* 29 (3), 641–656.
- Wiseman, H., Halliwell, B., 1996. Damage to DNA by reactive oxygen and nitrogen species: role in inflammatory disease and progression to cancer. *Biochem. J.* 313, 17–29, (PubMed: 8546679).
- Wolff, S., Crooks, L.E., Brown, P., Howard, R., Painter, R.B., 1980. Tests for DNA and chromosomal damage induced by nuclear magnetic resonance imaging. *Radiology* 136 (3), 707–710.
- Wong, C.G., Bottiglieri, T., Snead, O.C., III, 2003. GABA, gamma-hydroxybutyric acid, and neurological disease. *Ann. Neurol.* 54 (Suppl 6), S3–S12, (PubMed: 12891648).
- Xu, X., Yadav, N.N., Knutsson, L., Hua, J., Kalyani, R., Hall, E., Laterra, J., Blakeley, J., Strowd, R., Pomper, M., Barker, P., Chan, K., Liu, G., McMahon, M.T., Stevens, R.D., van Zijl, P.C., 2015. Dynamic glucose-enhanced (DGE) MRI: translation to human scanning and first results in glioma patients. *Tomography* 1, 105–114, (PubMed: 26779568).
- Yacoub, E., Harel, N., Uğurbil, K., 2008. High-field fMRI unveils orientation columns in humans. *Proc. Natl. Acad. Sci. USA* 105, 10607–10612, (PubMed: 18641121).
- Yanagisawa, Y., Nakagome, H., Hosono, M., Hamada, M., Kiyoshi, T., Hobo, F., Takahashi, M., Yamazaki, T., Maeda, H., 2008. Towards beyond-1GHz solution NMR: internal 2 H lock operation in an external current mode. *J. Mag. Reson.* 192, 329–337, (PubMed: 18424127).
- Zhu, X., Du, F., Zhang, N., Zhang, Y., Lei, H., Zhang, X., Qiao, H., Uğurbil, K., Chen, W., 2009. Advanced in vivo heteronuclear MRS approaches for studying brain bioenergetics driven by mitochondria. *Methods Mol. Biol.* 489, 317–357, (PubMed: 18839099).
- Zhu, X.H., Merkle, H., Kwag, J.H., Uğurbil, K., Chen, W., 2001. 17O relaxation time and NMR sensitivity of cerebral water and their field dependence. *Magn. Reson. Med.* 45, 543–549, (PubMed: 11283979).
- Zhu, X.H., Zhang, N., Zhang, Y., Zhang, X., Uğurbil, K., Chen, W., 2005. In vivo 17O NMR approaches for brain study at high field. *NMR Biomed.* 18, 83–103, (PubMed: 15770611).
- Zimmermann, J., Goebel, R., De Martino, F., van de Moortele, P.-F., Feinberg, D., Adriany, G., Chaïmow, D., Shmuel, D., Uğurbil, K., Yacoub, E., 2011. Mapping the organization of axis of motion selective features in human area MT using high-field fMRI. *PLoS One* 6, e28716, (PubMed: 22163328).